CHAPTER 4

TRANSIENT SATURATED FLOW BOILING OF FC-72 OVER A SMALL HEATED COPPER PLATE

The results obtained in the first part of the study are presented in this chapter to illustrate how the FC-72 mass flux oscillation affects the transient saturated flow boiling heat transfer of FC-72 over a small heated circular copper flat plate flush mounted on the bottom of a horizontal rectangular channel. The present experiments are carried out for the mean FC-72 mass flux fixed at 300 and 400 kg/m^2s for the imposed heat flux varying from 0.1 W/cm^2 to 10 W/cm^2. Besides, the amplitude of the coolant mass flux oscillation is set at 0%, 5% and 10% of the mean coolant mass flux. Moreover, the period of the mass flux oscillation is fixed at 10, 20 and 30 seconds. The coolant in the test section is at slightly subatmospheric pressure of 99 kPa with $T_{sat} = 55^{o}C$ for FC-72. In the following, the effects of the mean level, oscillation amplitude and period of the coolant mass flux, and the imposed heat flux on the transient FC-72 saturated flow boiling heat transfer performance are examined in detail. Note that for the limiting case of 0% mass flux oscillation for a given coolant mass flux we have saturated boiling of FC-72 at a coolant mass flux rate in the test section, which is designated as stable flow boiling. The heat transfer performance is presented mainly in terms of the transient variations of the average surface temperature of the copper plate and the boiling heat transfer coefficient.

4.1 Single-phase Liquid Convective Heat Transfer

Before beginning the two-phase flow boiling experiments, steady single-phase convective heat transfer experiments are conducted for liquid FC-72 flow in the rectangular channel. The measured average heat transfer coefficients for single-phase convection from the heated copper surface to the coolant are compared with the correlation proposed by Gersey and Mudawar [8]. The correlation of Gersey and Mudawar [8] is

$$\overline{Nu}_L = 0.362 \cdot Re_L^{0.614} \cdot Pr^{1/3} \tag{4.1}$$

where

$$Re_L = \frac{G \cdot L}{\mu_l} \tag{4.2}$$

$$\bar{h}_{1\phi} = \frac{k_l}{L} \cdot \overline{Nu}_L \tag{4.3}$$

for the flow velocity ranging from 13 cm/s to 400 cm/s. Their correlation is based on the experimental data procured from the same liquid and same flow configuration as the present data and the comparison is shown in Fig. 4.1 for the dimensional and dimensionless heat transfer coefficients. The results indicate that our data are in good agreements with their correlation.

It should be mentioned that all of the working fluid properties used in reducing the data for Fig. 4.1 from Equations 4.1 - 4.3 are calculated at the coolant inlet temperature. The copper plate diameter is chosen as the characteristic length in defining the Reynolds number Re_L and average Nusselt number $\overline{Nu}_L$ because of its significant effect on the heat transfer performance [8].

4.2 Stable and Time-average Saturated Flow Boiling Curves and Heat Transfer Coefficient

To illustrate the effects of the mass flux oscillation on the boiling characteristics, data for the FC-72 saturated flow boiling for a constant coolant mass flux are first compared with the time-average data for a transient oscillatory coolant mass flux. The results from this comparison are shown in Figures 4.2 and 4.3 by presenting the boiling curves for various mean mass fluxes and amplitudes and periods of the mass flux oscillation. Note that for each boiling curve at a given G the mean temperature of the copper plate increases gradually with the imposed heat flux at a low q from the saturated temperature of the coolant to a certain value just slightly higher than T_{sat} and no bubble nucleation is observed. The heat transfer in this region is completely due to the single-phase forced convection. With the continuing increase in the surface heat flux, bubbles begin to appear on the surface and the boiling curve is characterized by a sharp increase in the surface heat flux for a small rise in the temperature of copper surface. We have onset of nucleate boiling (ONB) in the flow. The reason causing the sharp increase in the slope of the boiling curve is due to a significant increase in the surface heat transfer by the boiling processes when ONB occurs. For the cases with oscillating coolant mass fluxes the ONB locations marked in these plots are the time-average values. Note that beyond ONB the coolant mass flux has slight effects on the boiling curves, suggesting that the surface heat transfer is mainly dominated by the fully developed nucleate boiling. Besides, at a higher G the required heat flux for ONB is higher and this implies that more energy is needed for the vapor to nucleate from the wall since the residence time of the coolant on the heated surface is shorter. It can be concluded from the results in Figures 4.2 and 4.3 that the time-average boiling curves are not affected by the amplitude and period of the coolant mass flux oscillation to a significant degree.

We move further to explore how the stable and transient time-average saturated flow boiling heat transfer coefficients $h_{2\phi,sat}$ are affected by the FC-72 coolant mass flux oscillation. The results for the variations of the time-average $h_{2\phi,sat}$ with the surface heat flux presented in Figures 4.4 and 4.5 reveal that the coolant mass flux oscillation amplitude and period show negligible influences on the time-average flow boiling heat transfer coefficients. However, for a given coolant mass flux the boiling heat transfer coefficient increases substantially with the imposed heat flux. For example, at T_{sat} =55^{o}C and $\overline{G}$ =400 kg/m^{2}s, the saturated boiling heat transfer coefficient for q =9.7 W/cm^2 is about 102% higher than that for q =3.2 W/cm^2 (Figure 4.4(a)).

4.3 Transient Flow Boiling Heat Transfer Characteristics

The transient boiling heat transfer characteristics for FC-72 flow over the heated copper plate resulting from the temporal coolant mass flux oscillation are illustrated by presenting the time variations of the space-average heated surface temperature T_w and heat transfer coefficient $h_{2\phi}$ for various imposed heat fluxes and mass fluxes. For comparison purpose the results for T_w for the limiting cases of constant coolant mass fluxes are shown in Figure 4.6. These data indicate that the fluctuations of the average heated surface temperature with time for various q and G are relatively small. The boiling can be regarded as at a statistically stable state.

Now when the coolant mass flux oscillates periodically in time in a form of nearly a triangular wave, significant temporal oscillations in the space average heated surface temperature occur for the imposed heat flux slightly higher than that for the time average ONB, as evident from the data shown in Figures 4.7 – 4.18 for the oscillation amplitude being 5% and 10% of the mean mass flux. Note that the temporal oscillation of the heated surface temperature is also periodic in time and is at the same frequency as the mass flux. Besides, the T_w oscillation gets stronger for higher imposed heat flux and higher amplitude of the mass flux oscillation. However, the period of the mass flux oscillation only slightly affects the T_w oscillation. It is of interest to note that at a higher amplitude of the mass flux oscillation with $\triangle G$ being 10% of $\overline{G}$, even in the single-phase forced convection the space average heated surface temperature also oscillates noticeably with time at a relatively low imposed heat flux with $q < \overline{q}_{ONB}$ (Figures 4.13 – 4.18). Here $\overline{q}_{ONB}$ is the time-average heat flux for ONB for the cases with the oscillating mass flux. But for the imposed heat flux around $\overline{q}_{ONB}$ the T_w oscillation is small for most cases except for $\overline{G}$=300 kg/m^{2}s with an intermediate period of the G oscillation at 20 seconds (Figure 4.15). A close inspection of the data given in Figures 4.7 – 4.18 further reveals that the T_w oscillation slightly lags the mass flux oscillation. Moreover for q substantially above $\overline{q}_{ONB}$ and in the period of time at which the instantaneous mass flux is higher than the average level, the space average heated surface temperature is higher than the corresponding time-average level, suggesting that the flow boiling heat transfer over the heated surface is poorer at a higher instantaneous G. But in the single-phase region the opposite is the case (Figures 4.13 - 4.15 and 4.17 – 4.18). The trend for the single-phase flow is apparently due to the better convection heat transfer for a higher mass flux. This somewhat unusual trend for the boiling flow requires more investigation into the bubble characteristics which will be examined later.

The corresponding time variations of the space-average flow boiling heat transfer coefficient affected by the coolant mass flux oscillation are shown in Figures 4.19 – 4.30. The results manifest that the flow boiling heat transfer coefficients also oscillate periodically in time and at the same frequency as the G oscillation. At a higher imposed heat flux and for the larger amplitude in the mass flux oscillation, the boiling heat transfer coefficients oscillate stronger. Besides in the period of time at which the mass flux is higher than the mean level, the space average boiling heat transfer coefficient is below the corresponding time-average level. Moreover, the oscillation in

$h_{2\phi}$ also lags slightly behind the mass flux oscillation.

In this transient oscillatory boiling flow the time variation of the coolant pressure at the inlet of the test section is also of interest in thermal-fluid design. These data are shown in Figures 4.31 – 4.42 for various cases. The results indicate that the inlet coolant pressure oscillates nearly in phase with the mass flux oscillation. Note that the inlet coolant pressure oscillation becomes somewhat irregular for the larger amplitude of the mass flux oscillation and a higher average mass flux (Figures 4.36, 4.38, 4.40 and 4.42). Finally, the quantitative data evaluated from the above results are summarized in Table 4.1 for the relative oscillation amplitudes of the space average heated surface temperature and boiling heat transfer coefficient $A_{T_w}/\Delta\overline{T}_{sat}$ and $A_{h2\varphi}/\overline{h}_{2\varphi}$ at various imposed heat fluxes and the amplitude and period of the coolant mass flux oscillation.

4.4 Transient Bubble Characteristics in Saturated Flow Boiling

To elucidate the transient saturated flow boiling heat transfer characteristics, the data for the bubble characteristics of FC-72 obtained from the present flow visualization are examined in the following. The top views of the boiling flow in a small region around the geometric center of the heated surface for various coolant mass fluxes and imposed heat fluxes are shown in Figs. 4.43 - 4.67 for the transient saturated flow boiling. At first, the bubble characteristics for the limiting cases of constant mass fluxes are illustrated by the photos in Figure 4.43. It is noted in the flow visualization and the results in Figure 4.43 that the vapor bubbles begin to appear as the heated surface temperature exceeds the boiling incipient superheat. In the beginning, tiny bubbles are observed in the active nucleation sites. The bubbles grow and then detach from the heated surface with certain mean bubble departure diameters.

As the imposed heat flux increases, more bubbles are generated on more active nucleation sites and more bubbles detach from the heated surface. Besides, the detached bubbles tend to merge into larger bubbles. Note that the large bubbles become distorted and elongated as they slide on the heating surface. Moreover, at a higher mass flux the bubbles are smaller and the bubble coalescence is less significant.

Next, the bubble characteristics in the transient flow boiling are illustrated by presenting the photos of the boiling flow at eight selected time instants in a typical periodic cycle in Figures 4.44 – 4.67. In these figures the symbol " $t=t_o$ " signifies the time instant at which the instantaneous mass flux is at the mean level and starts to increase with time. The results indicate that for a given imposed heat flux and fixed mean level, amplitude and period of the mass flux oscillation the bubbles get smaller and become more dispersed in the period the instantaneous mass flux increases. The opposite processes take place when the instantaneous mass flux decreases with time. These changes of the bubble characteristics with the instantaneous mass flux become more significant for an increase in the amplitude of the mass flux oscillation (Figures 4.44 and 4.56 and Figures 4.46 and 4.58). It is of interest to note that the mean level of the mass flux oscillation exhibits significant influences on the bubble characteristics in the transient flow boiling, as evident from comparing the results in Figures 4.44 and 4.46. Besides, the bubble characteristics are only affected slightly by the period of the mass flux oscillation for the small mass flux oscillation amplitude of 5%. But for the large amplitude of the mass flux oscillation of 10% the bubbles are larger for the cases with longer period of the mass flux oscillation (Figures 4.56 and 4.60).

To quantify the bubble characteristics, the measured data for the time variations of the space-average bubble departure diameter and frequency and active nucleation site density in a typical periodic cycle are given in Figs. 4.68 – 4.94 for various mean coolant mass fluxes, amplitudes and periods of the coolant mass flux oscillations, and imposed heat fluxes.

The results in Fig. 4.68(a) indicate that the mean size of the bubbles departing from the copper plate is somewhat smaller for the mass flux raised from 300 to 400 kg/m^2s in the stable flow boiling. It reflects the fact that the coolant at a higher mass flux and hence at a higher speed tends to sweep the bubbles more quickly away from the heating surface. Now as the coolant mass flux oscillates, the bubble departure diameter varies significantly with time (Figures 4.68(b) - (c)). More specifically, the size of the departing bubbles decreases in the first and fourth quarters of the periodic cycle in which the instantaneous mass flux increases with time. While in the second and third quarters of the cycle an opposite process is noted since the instantaneous mass flux decreases with time. Besides, at a higher imposed heat flux the departing bubbles are larger. Similar trend is noted in Figures 4.69 – 4.71. Comparing the results in Figure 4.68 with Figure 4.69 and Figure 4.70 with Figure 4.71 indicates that at the larger amplitude of the mass flux oscillation the effects of the imposed heat flux on the bubble departure diameter are somewhat smaller. The results in Figures 4.72 – 4.75 indicate that the bubble departure diameters are only affected slightly by the period of the mass flux oscillation.

Next, the data for the variations of the space-average bubble departure frequency with time for various cases are shown in Figures 4.77 – 4.80. In the stable flow boiling the increase in the bubble departure frequency with the imposed heat flux and coolant mass flux is clearly seen. The increase of f with G is ascribed again to the higher drag on the bubbles still attaching to the heated surface by the liquid coolant moving at a higher speed for a higher G. This, in turn, causes an earlier departure of the bubbles from the surface, resulting in a higher departure frequency. For an oscillation mass flux the bubbles depart from the heated surface at an increasing rate in the first and fourth quarters of the periodic cycle in which the coolant mass flux rises with time. Apparently, in the second and third quarters of the cycle in which G decreases the bubble departing rate reduces. It should be pointed out that the time variations of the bubble departure frequency are somewhat milder when compared with the bubble departure diameter. Figures 4.81 – 4.84 indicate that the bubble departure frequencies are only affected slightly by the period of the mass flux oscillation. The results shown in Figure 4.85 manifest that the mean level of the mass flux oscillation noticeably affects the bubble departure frequency.

Finally, the space-average active nucleation site density on the heated surface affected by the coolant mass flux oscillation is illustrated in Figures 4.86 – 4.89. The results in Figure 4.86(a) indicate that in stable flow boiling the active nucleation site density increases substantially with the imposed heat flux. But the increase is rather mild for the mass flux raised from 300 to 400 kg/m^2s. Note that in transient flow boiling the active nucleation site density decreases with time in the first and fourth quarters of the periodic cycle in which G increases. The reverse process appears in the second and third quarters of the cycle in which the coolant flow slows down. At the higher amplitude of the mass flux oscillation and at higher imposed heat flux the temporal variations of N_{ac} is stronger (Figures 4.88 and 4.89). The effects of the period of the mass flux oscillation on the time variations of N_{ac} are rather weak (Figures 4.90 – 4.93). The amplitude of the N_{ac} oscillation is slighter higher for a larger amplitude of the mass flux oscillation (Figure 4.94).

4.5 Correlation Equations

According to the present experimental data, empirical correlations for the space-average bubble departure diameters in FC-72 stable and transient saturated flow boiling on the heated circular copper flat plate flush mounted on the bottom of the rectangular channel estimated from the present flow visualization are proposed as

$$\frac{d_p}{\sqrt{\sigma/g\cdot\Delta\rho}} = \frac{0.2\cdot(\rho_l/\rho_v)^{0.48}\cdot\overline{Bo}^{0.21}}{\overline{Re_D}^{0.08}} \quad \text{for stable flow boiling} \qquad (4.4)$$

where $\overline{Re_D}$ and $\overline{Bo}$ are the mean Reynolds and Boiling numbers respectively. They are defined as

$$\overline{Re_D} = \frac{\overline{G}\cdot D}{\mu_l} \qquad (4.5)$$

$$\overline{Bo} = \frac{q''}{\overline{G}\cdot i_{lv}} \qquad (4.6)$$

and

$$\frac{d_p}{\sqrt{\sigma/g\cdot\Delta\rho}} = \frac{0.2\cdot(\rho_l/\rho_v)^{0.48}\cdot Bo^{0.22}}{Re_D^{0.08}} \quad \text{for transient flow boiling} \qquad (4.7)$$

where Re_D and Bo are respectively the instantaneous Reynolds and Boiling numbers. They are defined as

$$Re_D = \frac{G\cdot D}{\mu_l} \qquad (4.8)$$

$$Bo = \frac{q''}{G\cdot i_{lv}} \qquad (4.9)$$

where $G(=\overline{G}+\Delta G)$ is the instantaneous coolant mass flux, $\overline{G}$ is the average coolant mass flux, ΔG is the amplitude of the mass flux oscillation, ρ_l is the liquid density, and D is the copper plate diameter. Figures 4.95 and 4.96 show that the present experimental data fall within ±20 % of the correlations given in Equations (4.4) and (4.7). In addition, empirical equations are provided to correlate the data for the space-average bubble departure frequency as

$$\frac{f\cdot d_p}{\mu_l/\rho_l\cdot D_h} = 0.5\overline{Re_D}^{1.3}\cdot Pr^{0.7}\cdot\overline{Bo}^{0.66} \quad \text{for stable flow boiling} \qquad (4.10)$$

and

$$\frac{f\cdot d_p}{\mu_l/\rho_l\cdot D_h} = 0.5Re_D^{1.3}\cdot Pr^{0.7}\cdot Bo^{0.7} \quad \text{for transient flow boiling} \qquad (4.11)$$

Figures 4.97 and 4.98 reveal that the present experimental data for $f\cdot d_p$ can be correlated with the deviation less than ±20 % and ±25 % by the above two equations. Moreover, empirical correlations for the space-average active nucleation site density in the FC-72 saturated flow boiling deduced from the present flow visualization are proposed as

$$N_{ac} \cdot d_p^{\ 2} = -0.065 + (85 \cdot \overline{Bo}^{0.83} \cdot \overline{Re_D}^{-0.15}) \quad \text{for stable flow boiling} \tag{4.12}$$

and

$$N_{ac} \cdot d_p^{\ 2} = -0.03 + (45 \cdot Bo^{0.85} \cdot Re_D^{-0.13}) \quad \text{for transient flow boiling} \tag{4.13}$$

The comparison in Figs. 4.99 and 4.100 shows that more than 85 % of the present experimental data fall within ± 30 % and ± 40 % of the correlation given in Equations (4.12) and (4.13). Finally, the total heat flux input to the stable boiling flow q_t is considered to be roughly composed of two parts: one resulting from the bubble nucleation q_b and another due to the single phase forced convection q_c. Thus

$$q_t = q_b + q_c \tag{4.14}$$

Here q_b and q_c can be individually calculated from the quantitative data for the bubble characteristics examined in section 5.3 and single phase liquid forced convection as

$$q_b = \rho_v \cdot V_v \cdot f \cdot N_{ac} \cdot i_{lv} \tag{4.15}$$

where ρ_v is the vapor density, V_v is the vapor volume of the mean departing bubble defined as $\frac{4\pi}{3}(\frac{d_p}{2})^3$, f is the space-average bubble departure frequency, N_{ac} is the space-average active nucleation site density, i_{lv} is the enthalpy of vaporization, and

$$q_c = E \cdot \overline{h}_{l\phi} \cdot \Delta T_{sat} \tag{4.16}$$

where E is an enhancement factor added to account for the agitating motion of the bubbles which can enhance the single phase liquid convection heat transfer. From the experimental data, E can be empirically correlated as

$$E = 4.5 \cdot N_{conf}^{\ 0.5} \cdot \overline{Fr_l}^{-0.15} \cdot (1 + 280 \cdot \overline{Bo})^{1.8} \quad \text{for stable flow boiling} \tag{4.17}$$

Here $\overline{Fr_l}$ is the Froude number and N_{conf} is the Confinement number. They are respectively defined as

$$N_{conf} = \frac{(\sigma/g \cdot \Delta\rho)^{0.5}}{D_h} \tag{4.18}$$

and

$$\overline{Fr_l} = \frac{\overline{G}^2}{\rho_l^{\,2} \cdot g \cdot D_h} \tag{4.19}$$

where g is the acceleration due to gravity, D_h is the hydraulic diameter of the test section, and ΔT_{sat} (= T_w - T_{sat}) is the wall superheat. The results shown in Figure 4.101 indicate that the present data can be correlated with the deviation less than ± 25% by the empirical correlation given in Equations (4.14) - (4.19).

Table 4.1 Relative amplitudes of heated surface temperature and heat transfer coefficient oscillations in transient oscillatory saturated flow boiling for various imposed heat fluxes and the amplitudes and periods of the coolant mass flux oscillation.

$\Delta G/\overline{G}$	t_p (sec)	$\overline{G}$ =300 kg/m^{2}s			$\overline{G}$ =400 kg/m^{2}s		
		q(W/cm^2)	$A_{T_w}/\Delta\overline{T}_{sat}$	$A_{h_{2\varphi}}/\overline{h}_{2\varphi}$	q(W/cm^2)	$A_{T_w}/\Delta\overline{T}_{sat}$	$A_{h_{2\varphi}}/\overline{h}_{2\varphi}$
±5%	10	5.05	0.0097	0.0098	5.05	0.0099	0.0099
		6.23	0.0078	0.0078	6.24	0.0105	0.0105
		8.25	0.0095	0.0094	8.26	0.0096	0.0095
		9.74	0.0089	0.0088	9.74	0.0101	0.0100
	20	4.99	0.0098	0.0110	5.04	0.0179	0.0180
		6.18	0.0104	0.0128	6.18	0.0219	0.0221
		8.24	0.0083	0.0094	8.23	0.0153	0.0153
		9.75	0.0088	0.0087	9.76	0.0156	0.0156
	30	4.95	0.0084	0.0084	5.01	0.0182	0.0183
		6.15	0.0116	0.0116	6.16	0.0184	0.0184
		8.21	0.0094	0.0094	8.20	0.0141	0.0141
		9.70	0.0077	0.0077	9.72	0.0143	0.0144
±10%	10	5.04	0.0082	0.0082	5.03	0.0136	0.0136
		6.15	0.0153	0.0153	6.19	0.0178	0.0177
		8.17	0.0149	0.0149	8.20	0.0185	0.0185
		9.68	0.0151	0.0151	9.70	0.0185	0.0185
	20	4.95	0.0135	0.0135	4.99	0.0285	0.0285
		6.17	0.0177	0.0177	6.19	0.0280	0.0280
		8.21	0.0173	0.0173	8.22	0.0267	0.0267
		9.71	0.0185	0.0185	9.76	0.0230	0.0231
	30	4.94	0.0187	0.0188	5.02	0.0227	0.0227
		6.11	0.0189	0.0188	6.16	0.0226	0.0228
		8.18	0.0184	0.0184	8.20	0.0254	0.0256
		9.69	0.0184	0.0184	9.73	0.0252	0.0253

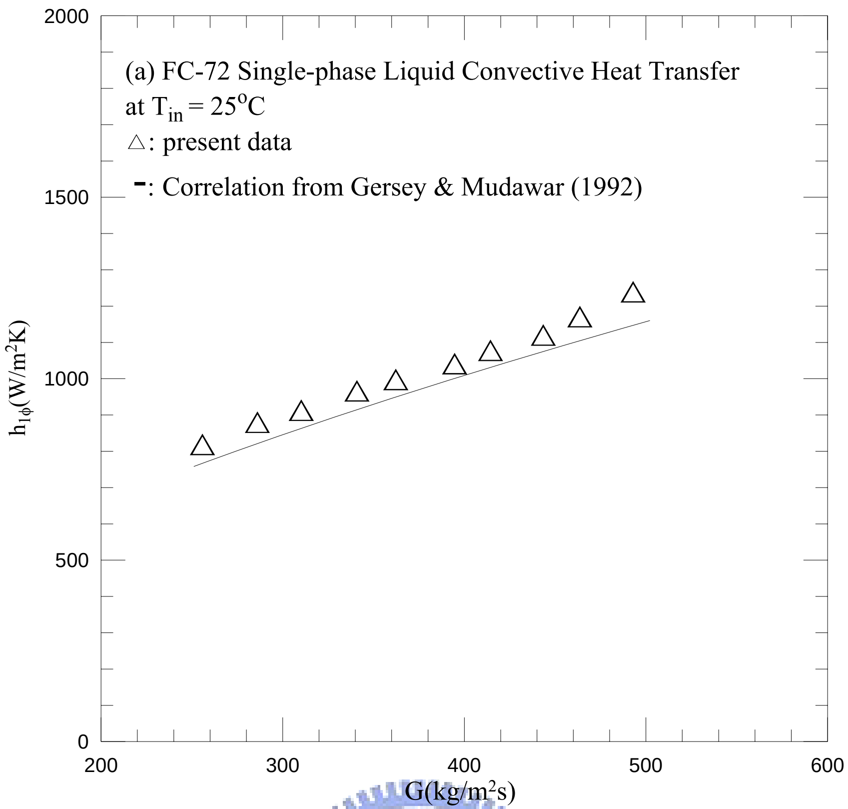

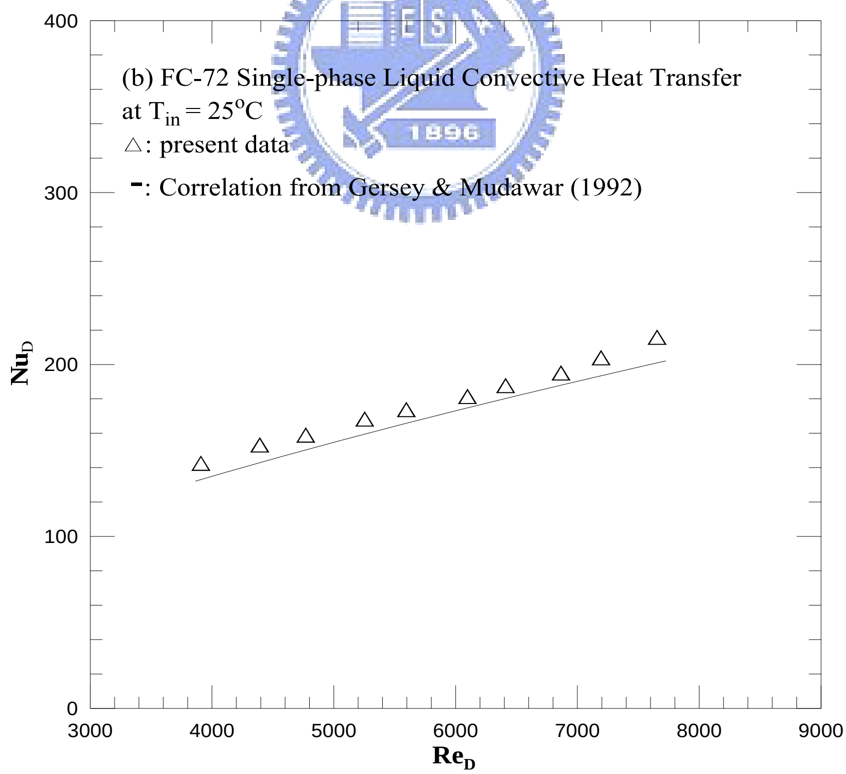

Fig. 4.1 Comparison of the present steady single-phase liquid convection heat transfer data with the correlation of Gersey and Mudawar (1992) for (a) $h_{1\phi}$ vs. G an (b) Nu_L vs. Re_L.

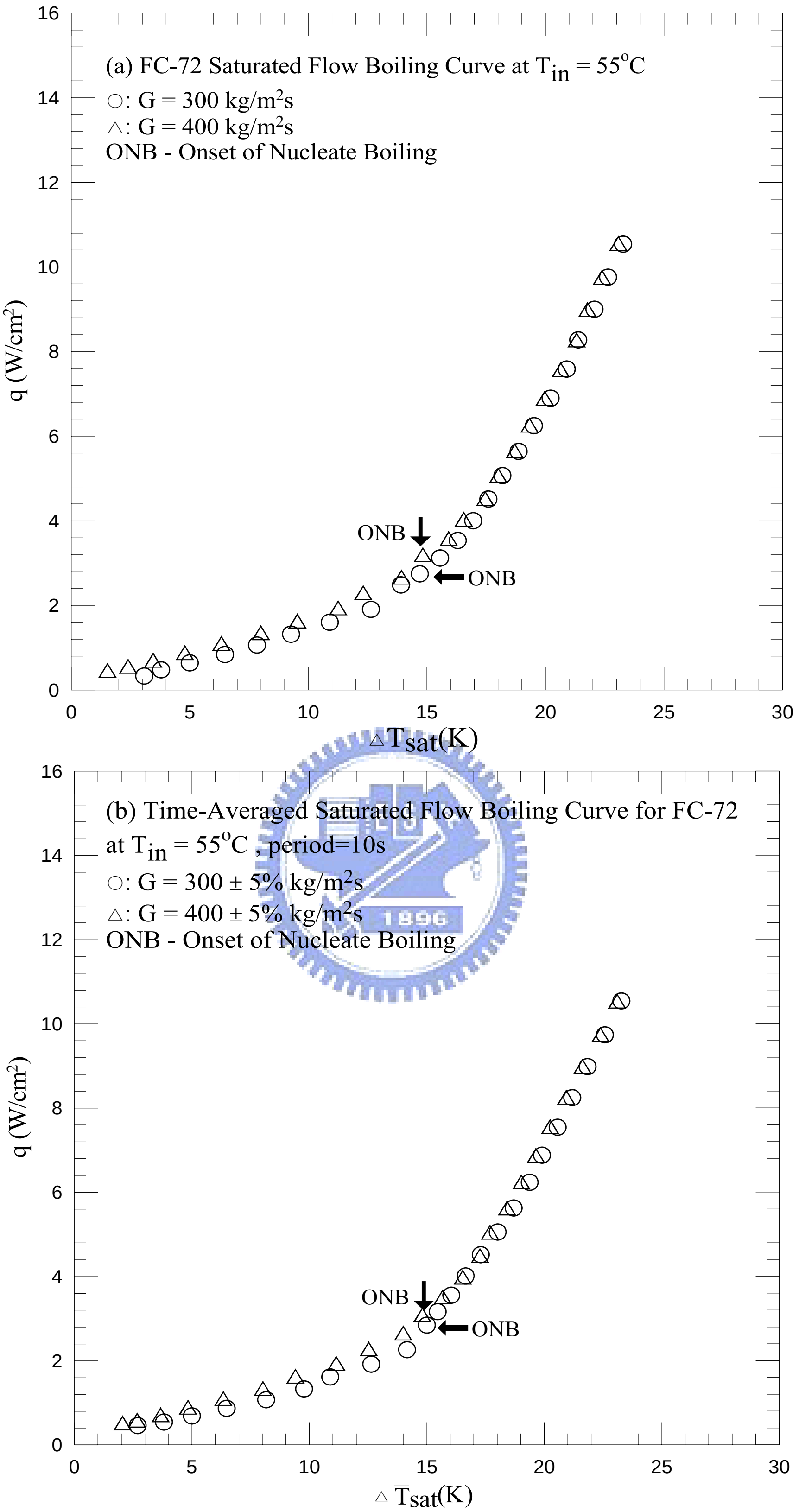

Fig. 4.2 Time-average flow boiling curves for various coolant mass fluxes for stable saturated flow boiling (a) and transient saturated flow boiling for t_p=10 sec (b), 20 sec (c) and 30 sec (d).

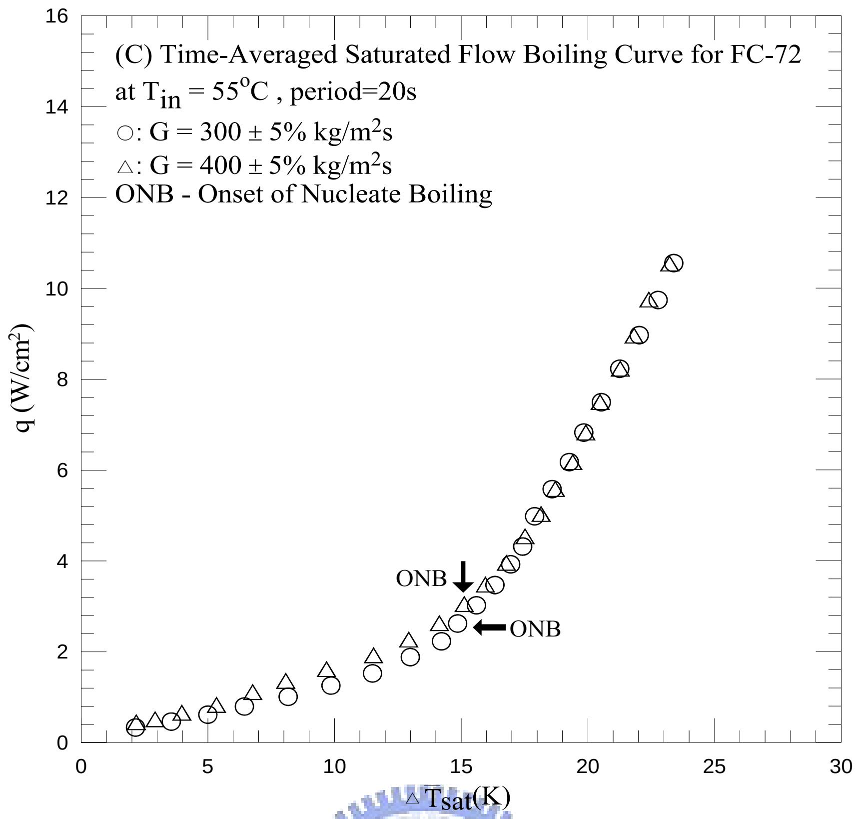

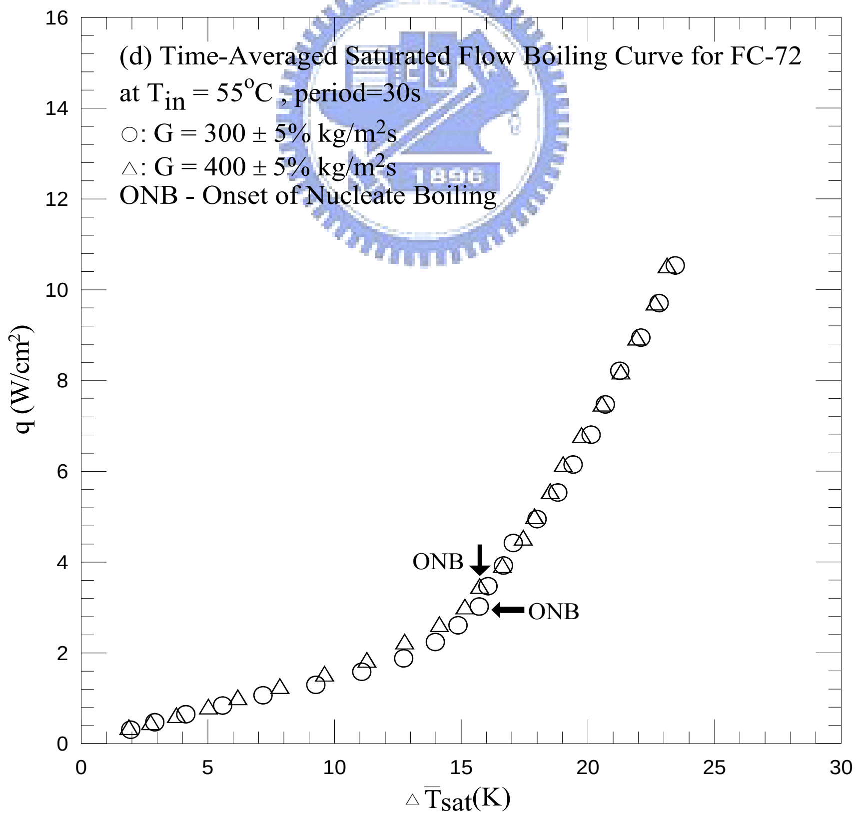

Fig. 4.2 Continued.

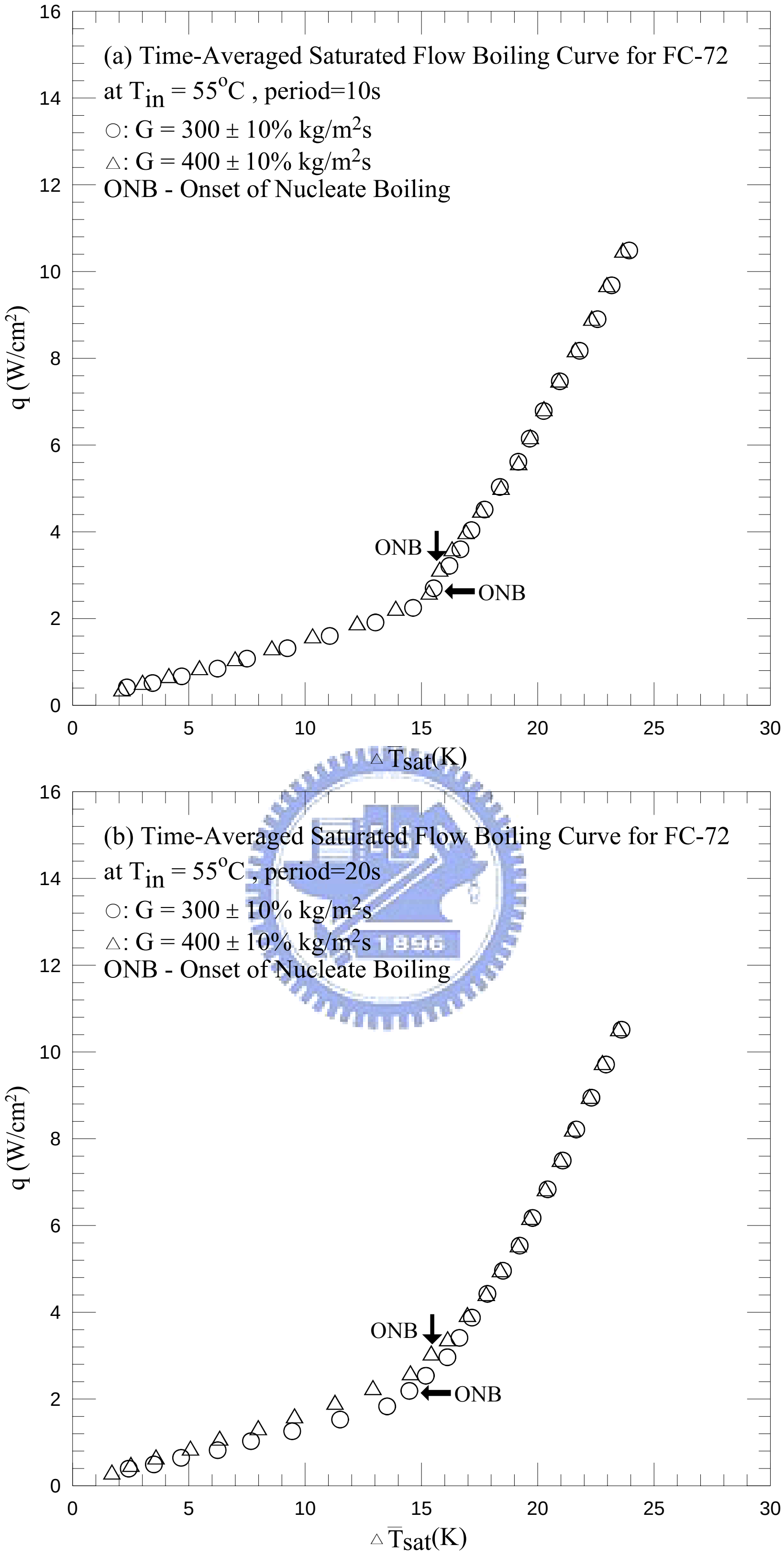

Fig. 4.3 Time-average flow boiling curves for various coolant mass fluxes for transient saturated flow boiling at t_p=10 sec (a), 20 sec (b) and 30 sec (c).

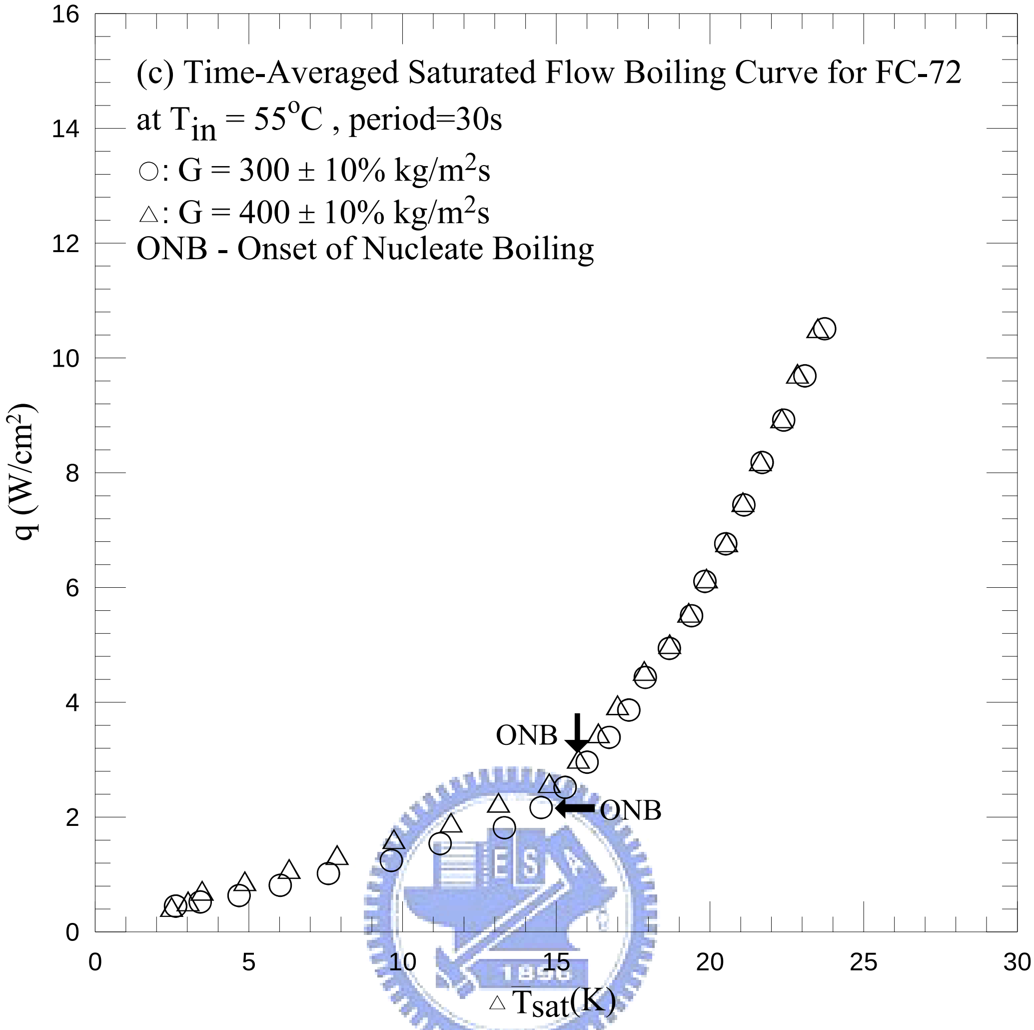

Fig. 4.3 Continued.

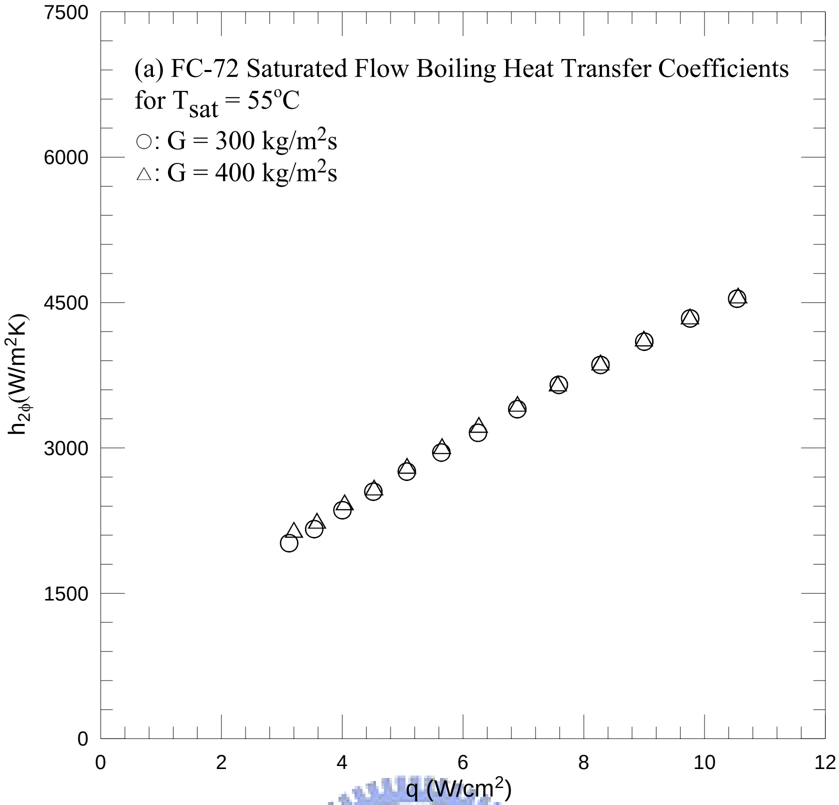

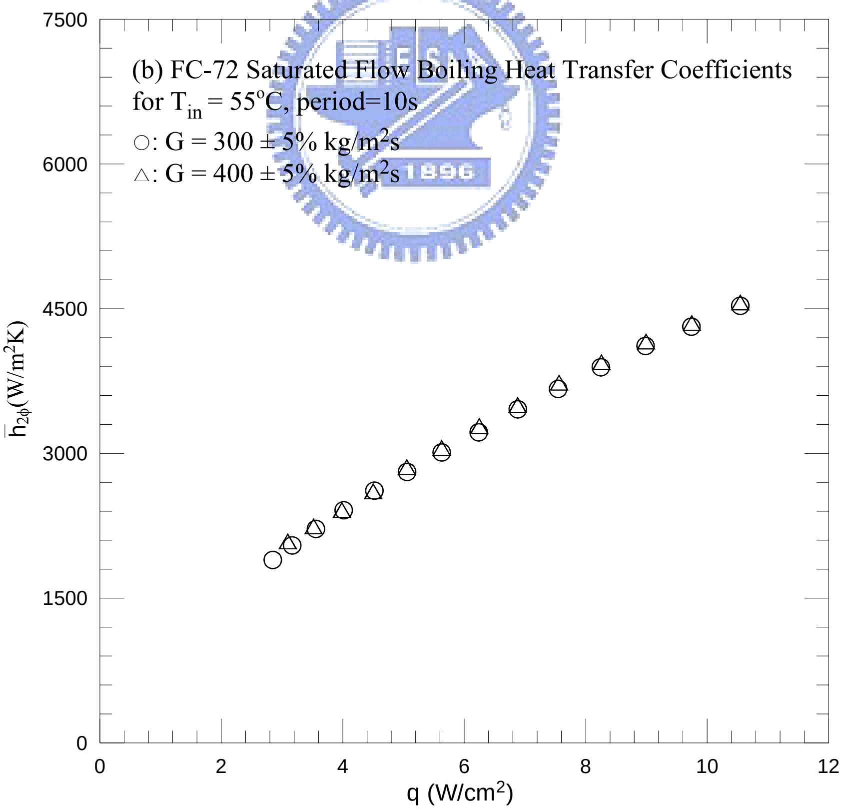

Fig. 4.4 Time-average flow boiling heat transfer coefficients for various coolant mass fluxes for stable saturated flow boiling (a) and transient saturated flow boiling at t_p=10 sec (b), 20 sec (c) and 30 sec (d).

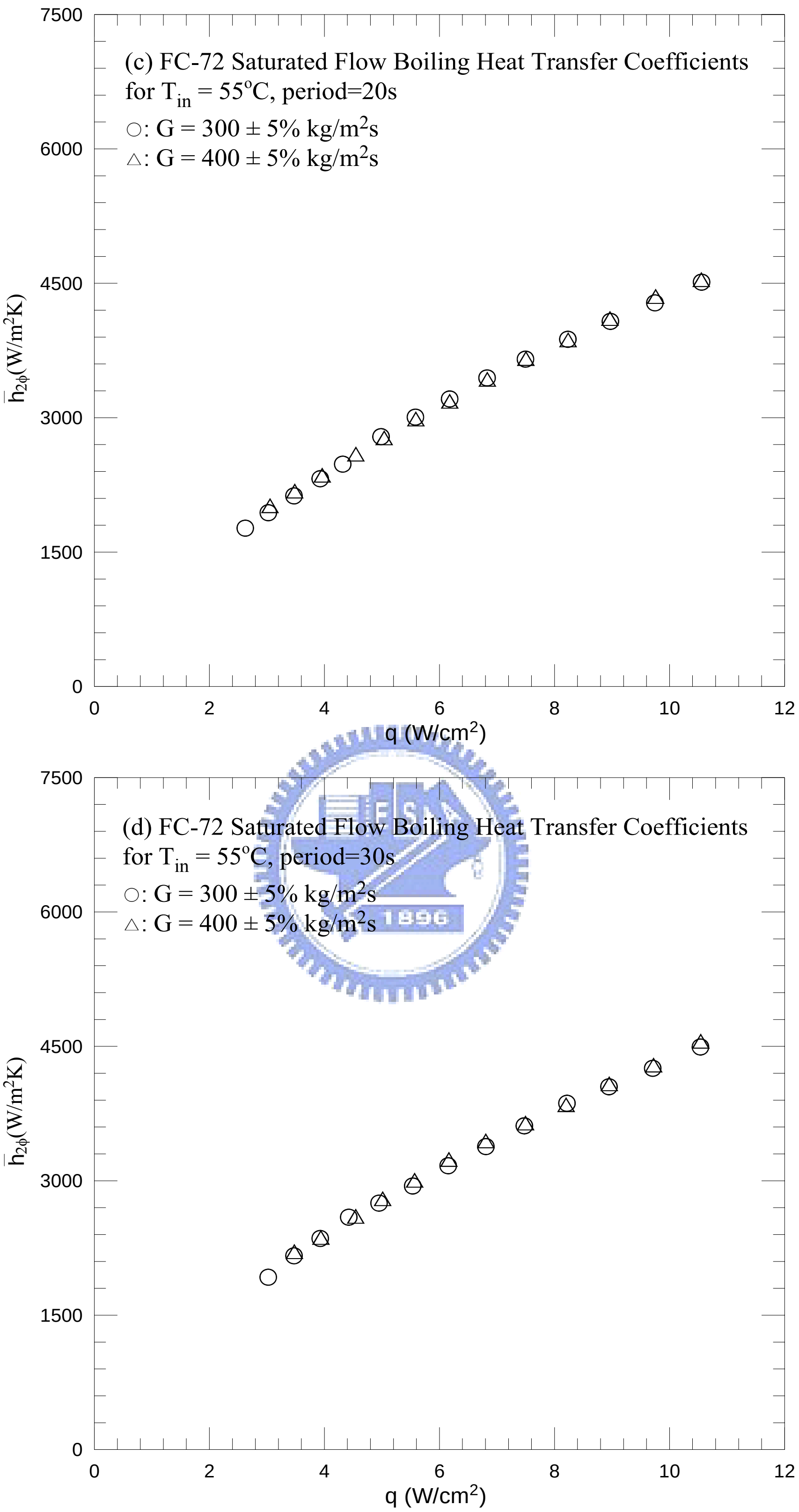

Fig. 4.4 Continued.

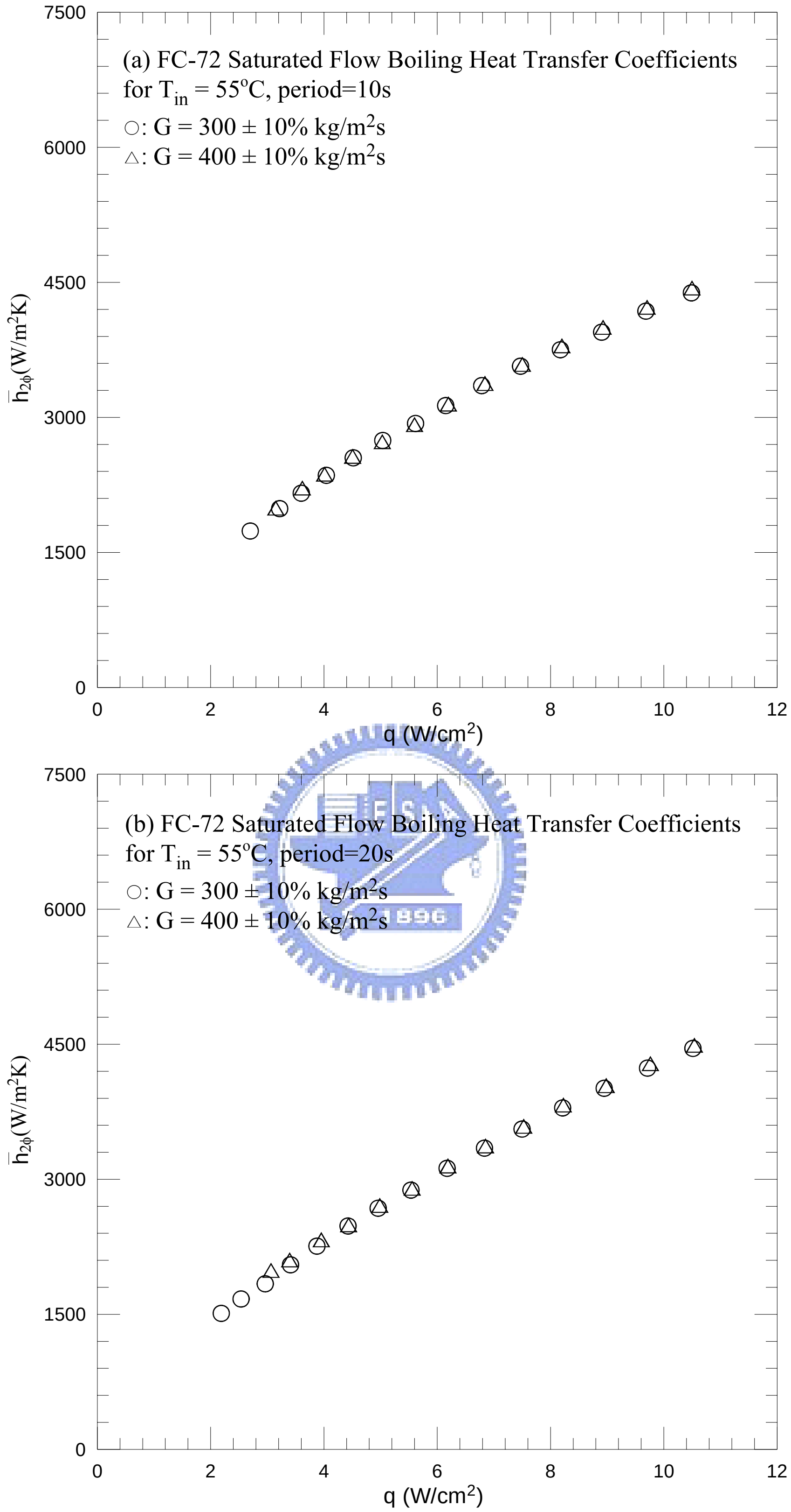

Fig. 4.5 Time-average flow boiling heat transfer coefficients for various coolant mass fluxes for transient saturated flow boiling at t_p=10 sec (a), 20 sec (b) and 30 sec (c).

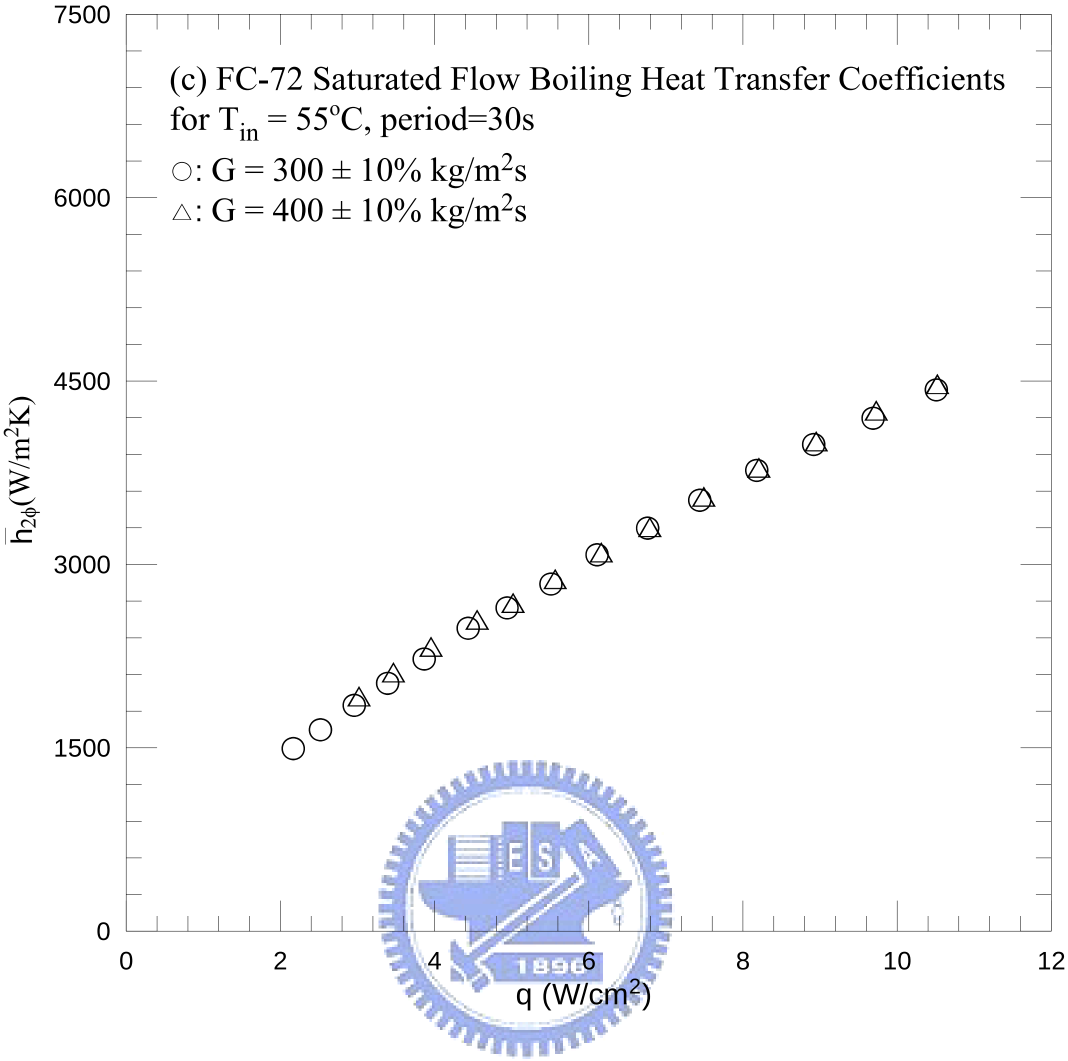

Fig. 4.5 Continued.

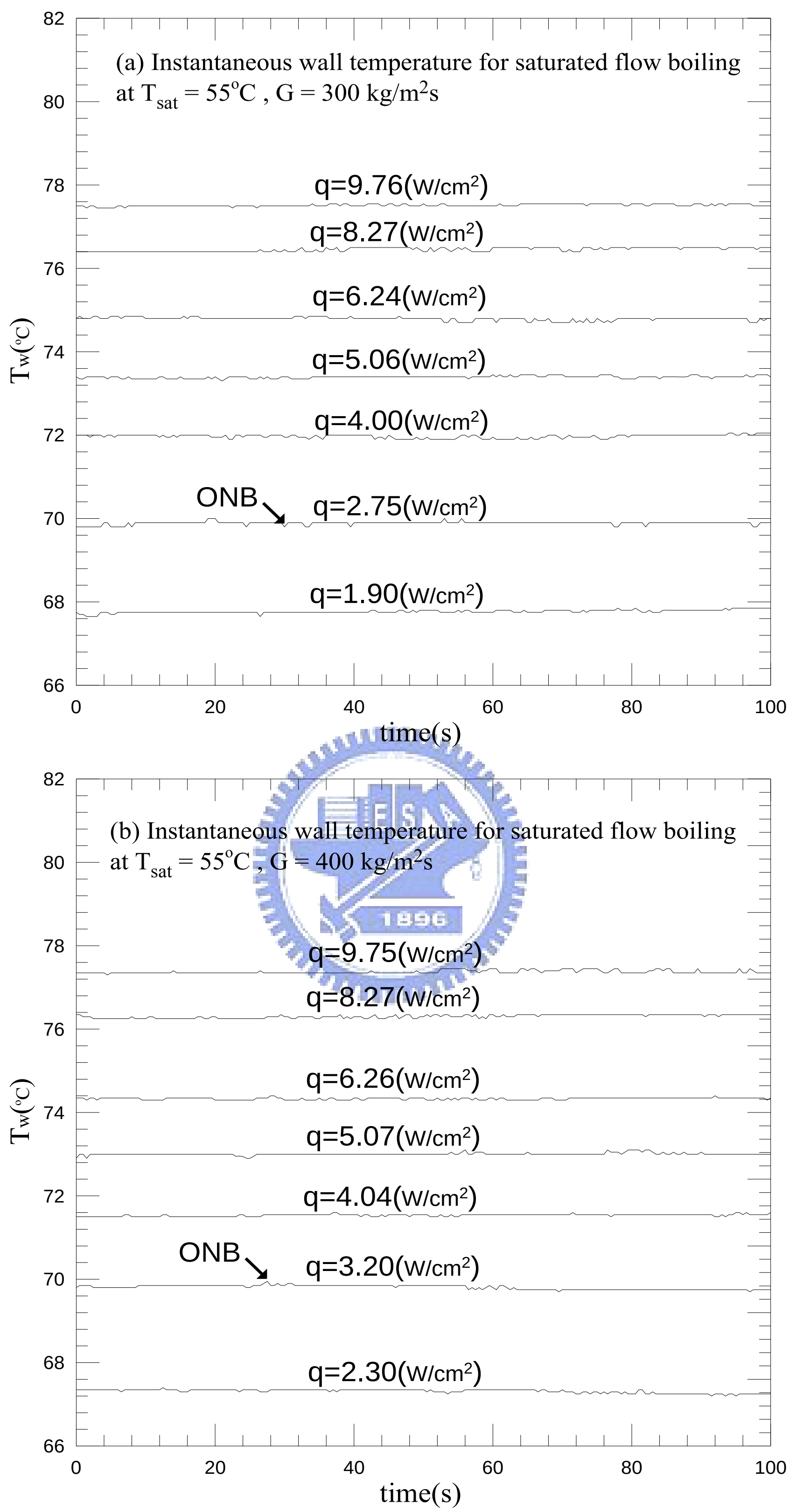

Fig. 4.6 Time variations of the copper plate temperature in stable saturated flow boiling for various imposed heat fluxes at (a) G=300 kg/m^{2}s and (b) G=400 kg/m^{2}s.

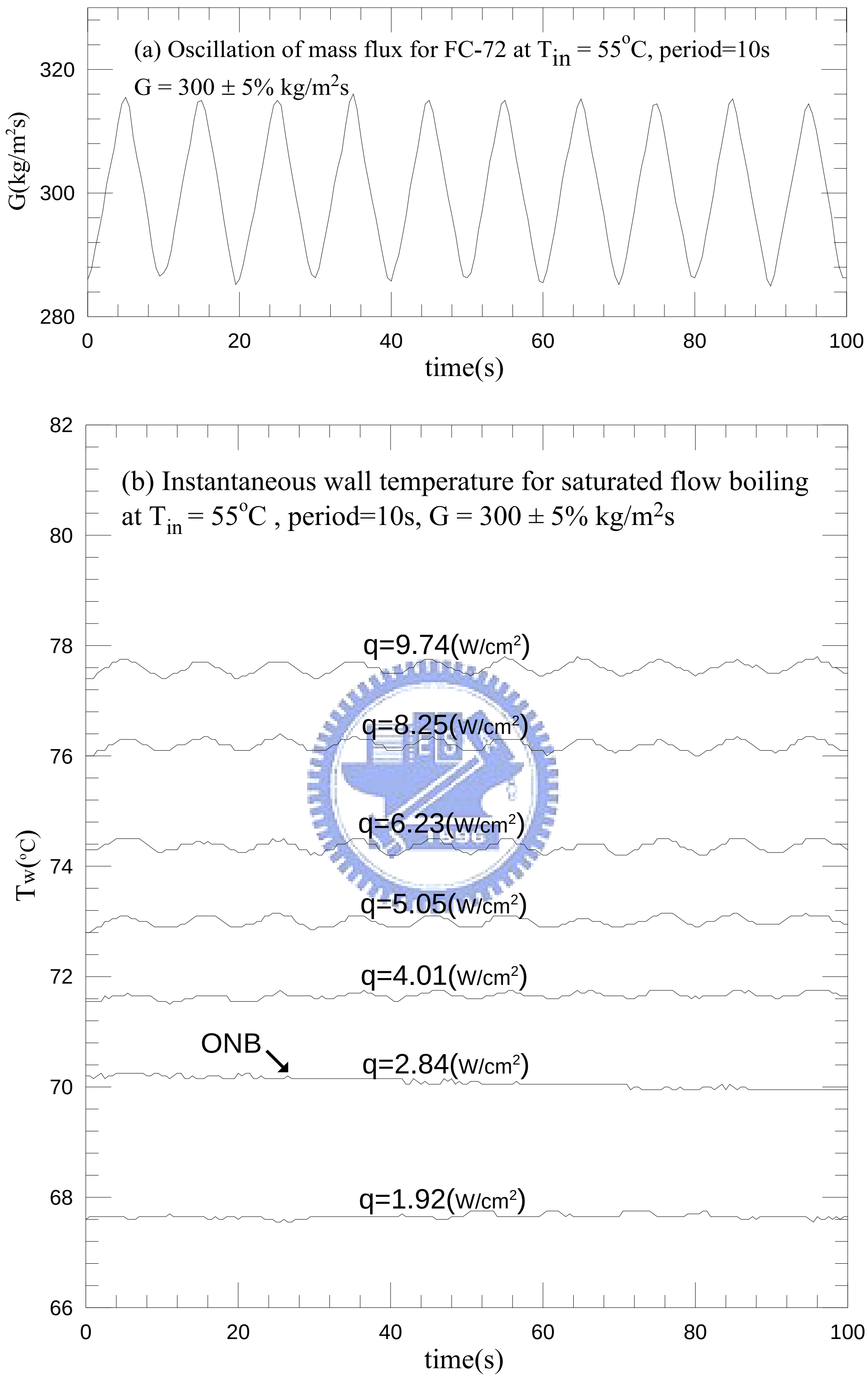

Fig. 4.7 Time variations of (a) imposed coolant mass flux and (b) copper plate temperature in transient oscillatory saturated flow boiling for various imposed heat fluxes for G=300±5% kg/m^{2}s with t_p=10 sec.($\overline{q}_{ONB}$ =2.84 w/cm^2 at G =300 kg/m^{2}s)

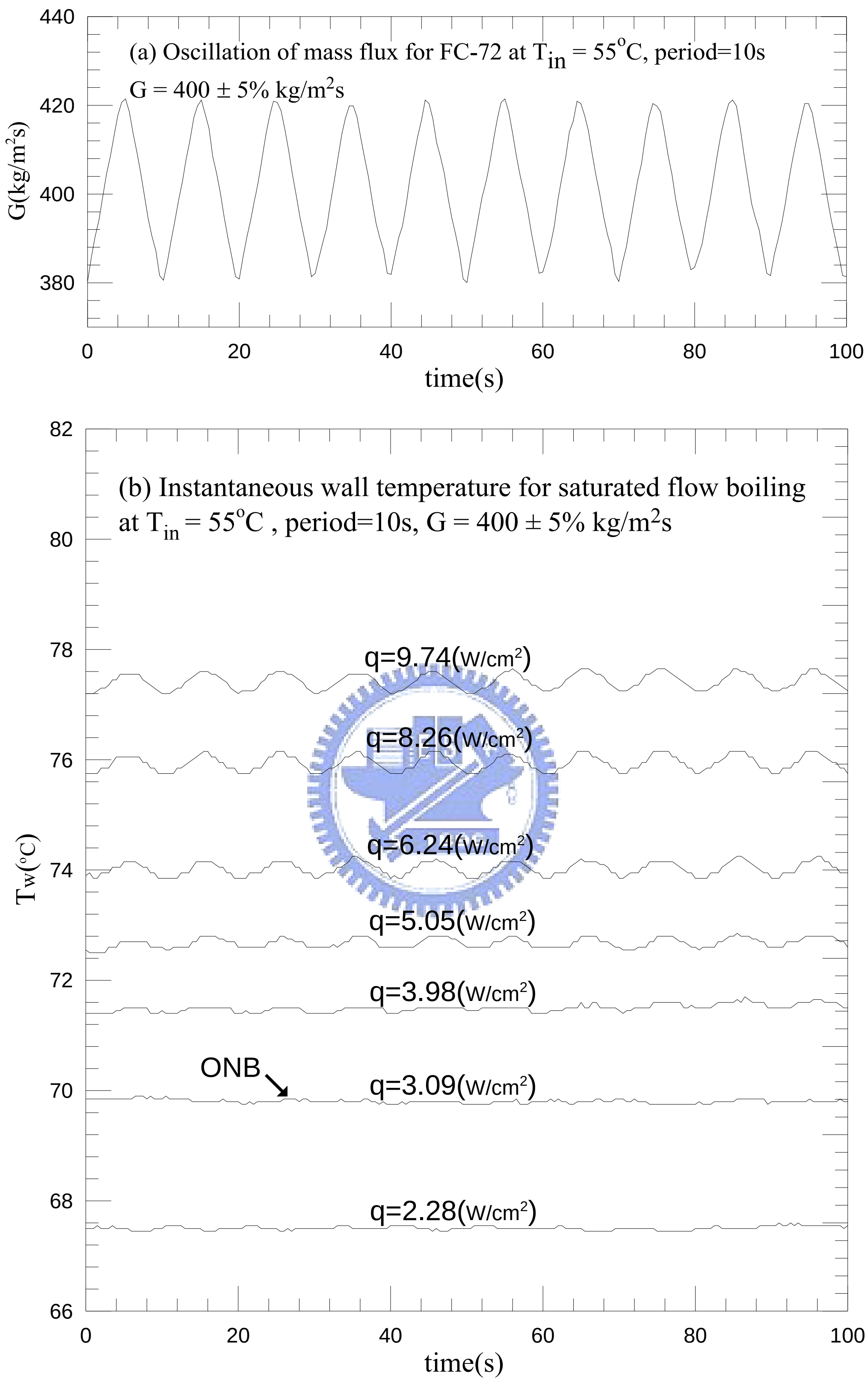

Fig. 4.8 Time variations of (a) imposed coolant mass flux and (b) copper plate temperature in transient oscillatory saturated flow boiling for various imposed heat fluxes for G=400±5% kg/m²s with t_p=10 sec.($\overline{q}_{ONB}$ =3.09 w/cm² at G =400 kg/m²s)

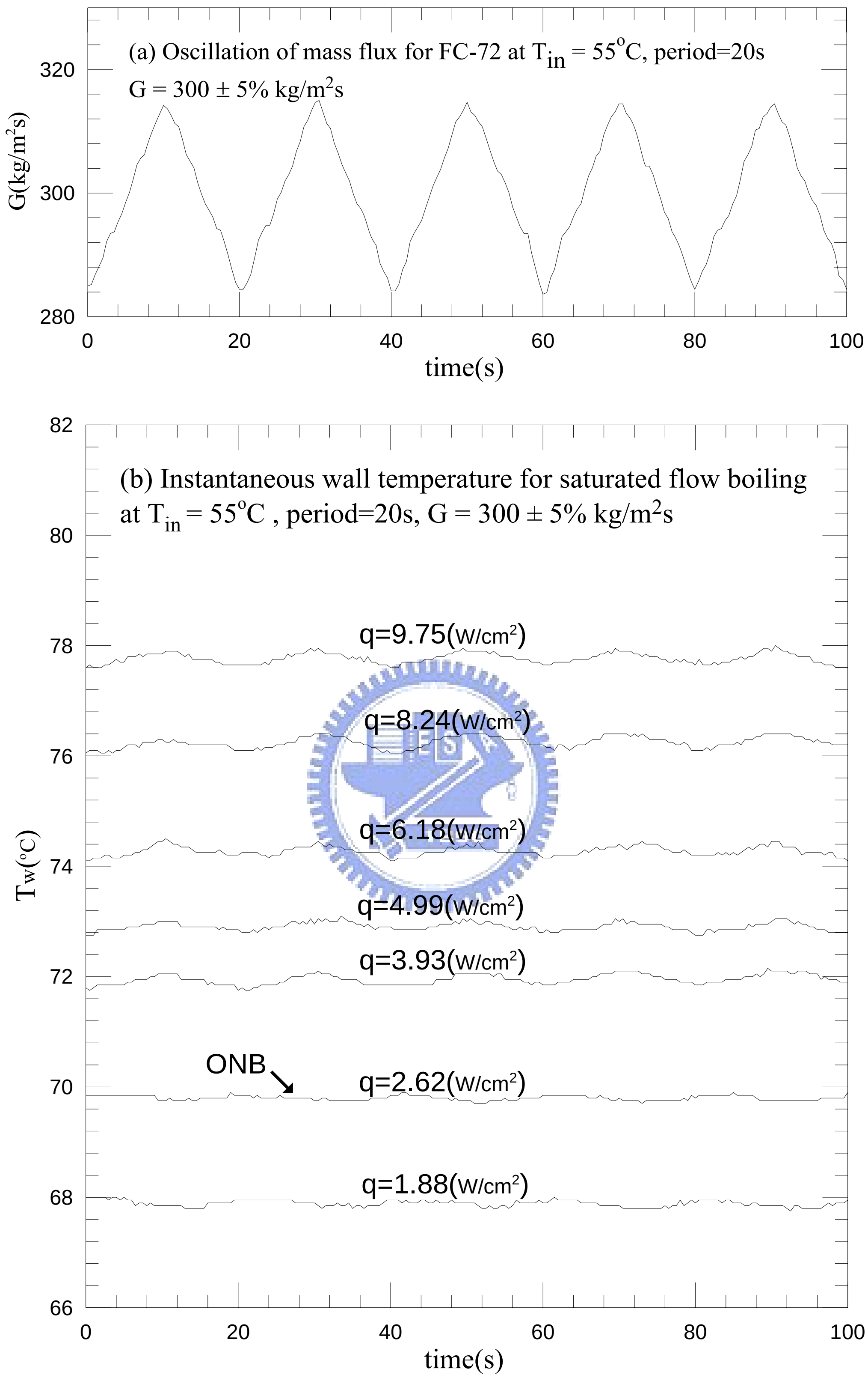

Fig. 4.9 Time variations of (a) imposed coolant mass flux and (b) copper plate temperature in transient oscillatory saturated flow boiling for various imposed heat fluxes for G=300±5% kg/m^{2}s with t_p=20 sec.($\overline{q}_{ONB}$ =2.62 w/cm^2 at G =300 kg/m^{2}s)

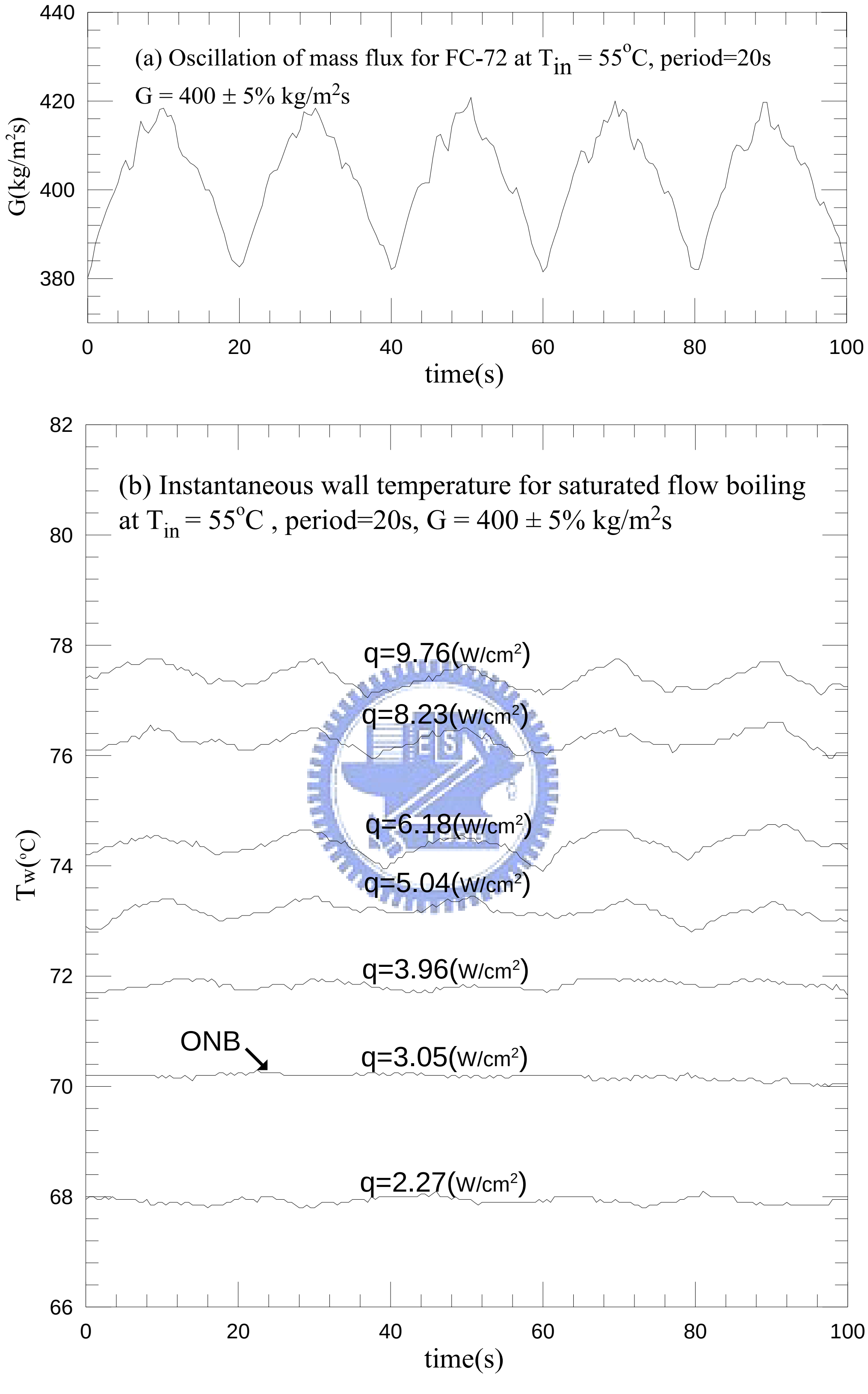

Fig. 4.10 Time variations of (a) imposed coolant mass flux and (b) copper plate temperature in transient oscillatory saturated flow boiling for various imposed heat fluxes for G=400±5% kg/m^{2}s with t_p=20 sec.($\overline{q}_{ONB}$=3.05 w/cm^2 at G =400 kg/m^{2}s)

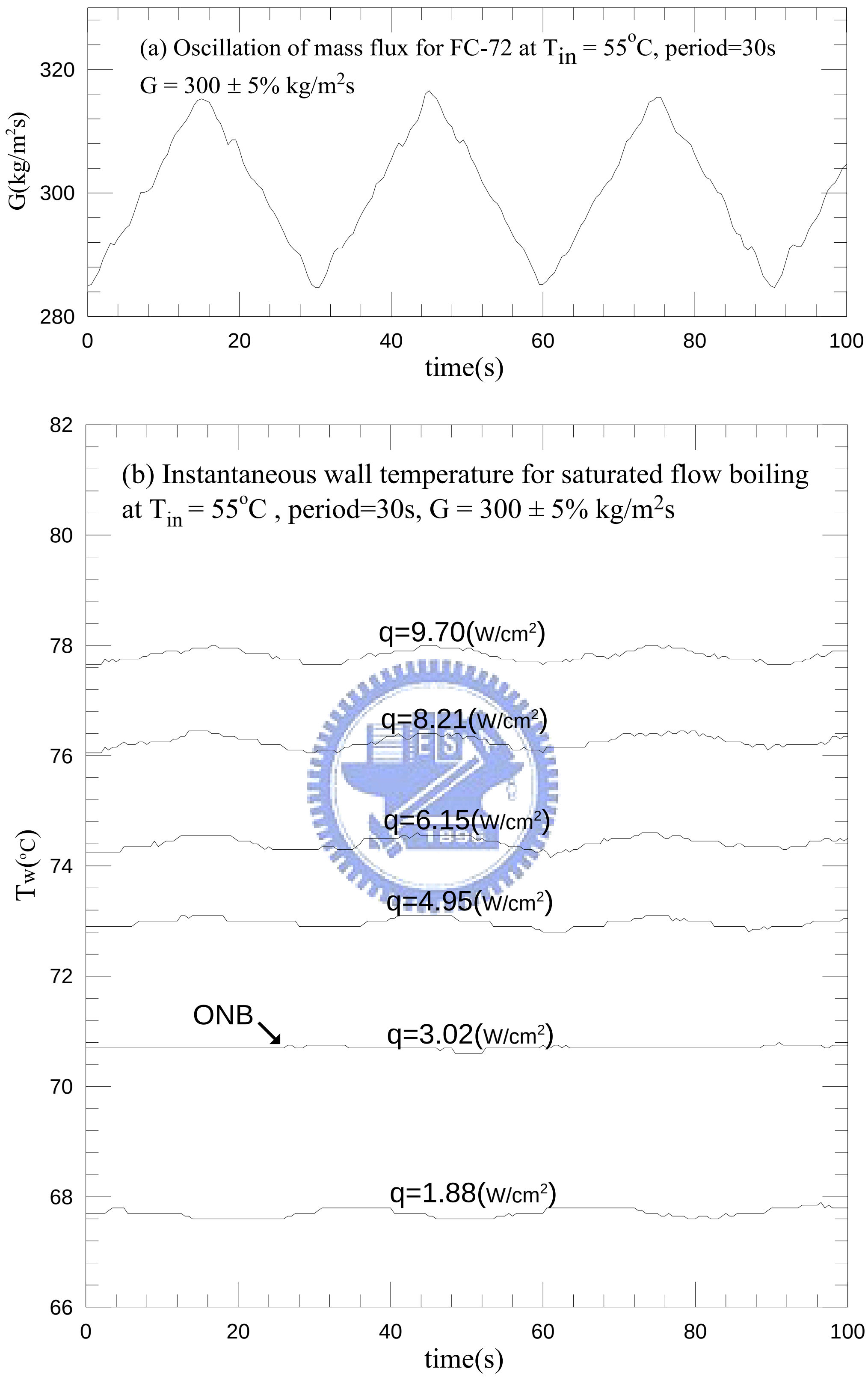

Fig. 4.11 Time variations of (a) imposed coolant mass flux and (b) copper plate temperature in transient oscillatory saturated flow boiling for various imposed heat fluxes for G=300±5% kg/m^{2}s with t_p=30 sec.($\overline{q}_{ONB}$ =3.02 w/cm^2 at G =300 kg/m^{2}S)

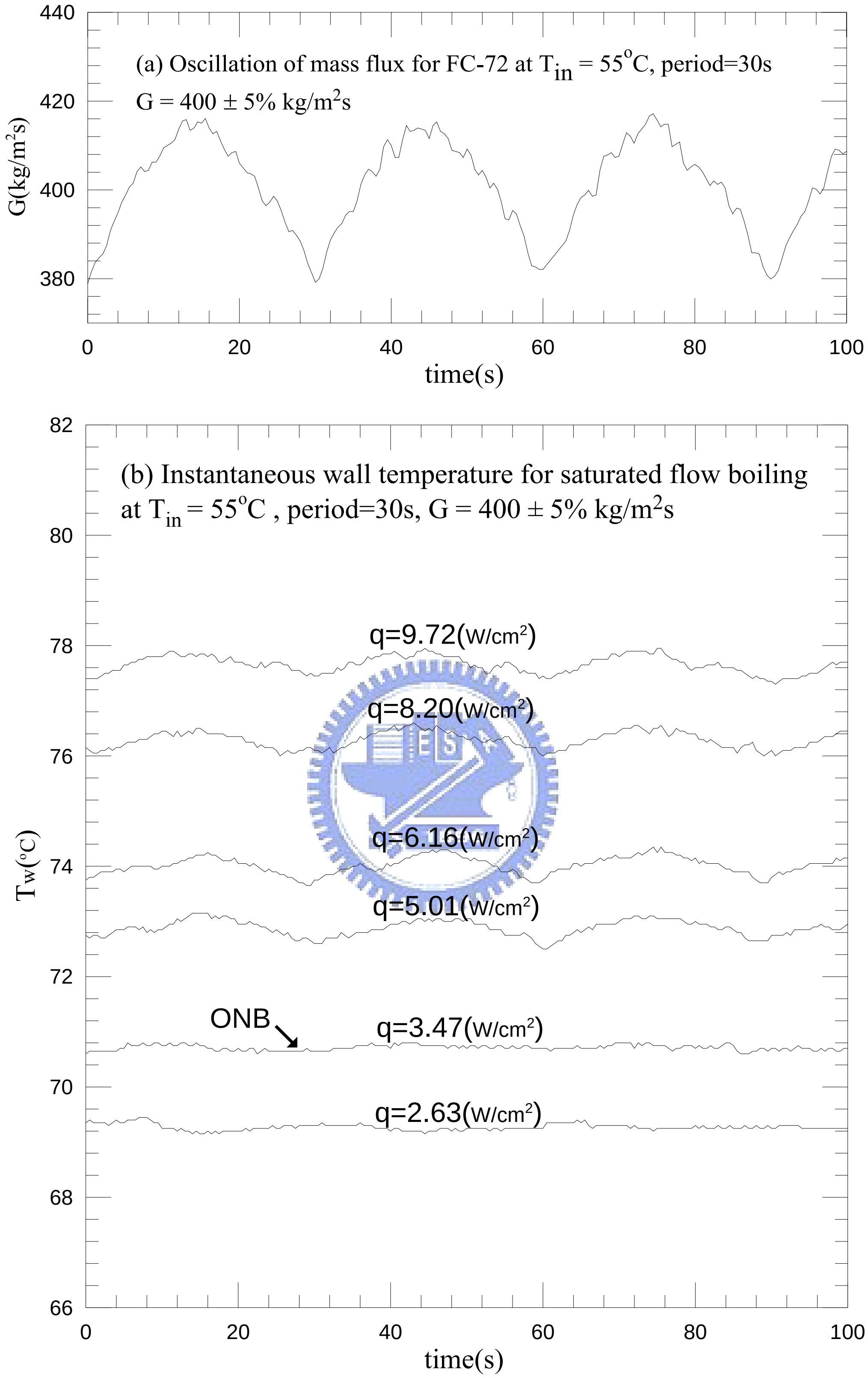

Fig. 4.12 Time variations of (a) imposed coolant mass flux and (b) copper plate temperature in transient oscillatory saturated flow boiling for various imposed heat fluxes for G=400±5% kg/m²s with t_p=30 sec.($\overline{q}_{ONB}$ =3.47 w/cm² at G =400 kg/m²s)

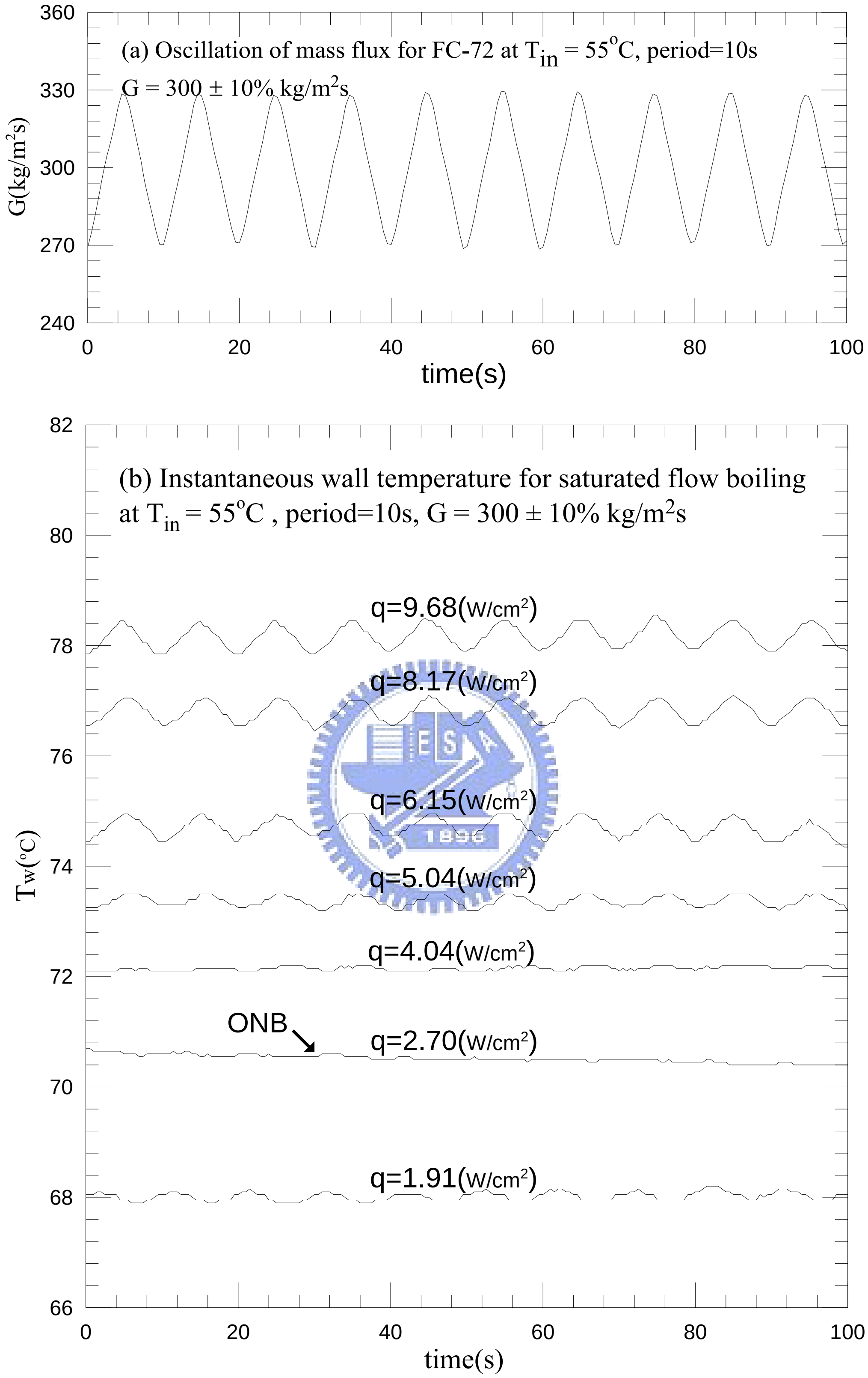

Fig. 4.13 Time variations of (a) imposed coolant mass flux and (b) copper plate temperature in transient oscillatory saturated flow boiling for various imposed heat fluxes for G=300±10% kg/m^{2}s with t_p=10 sec.($\overline{q}_{ONB}$ =2.70 w/cm^2 at G =300 kg/m^{2}S)

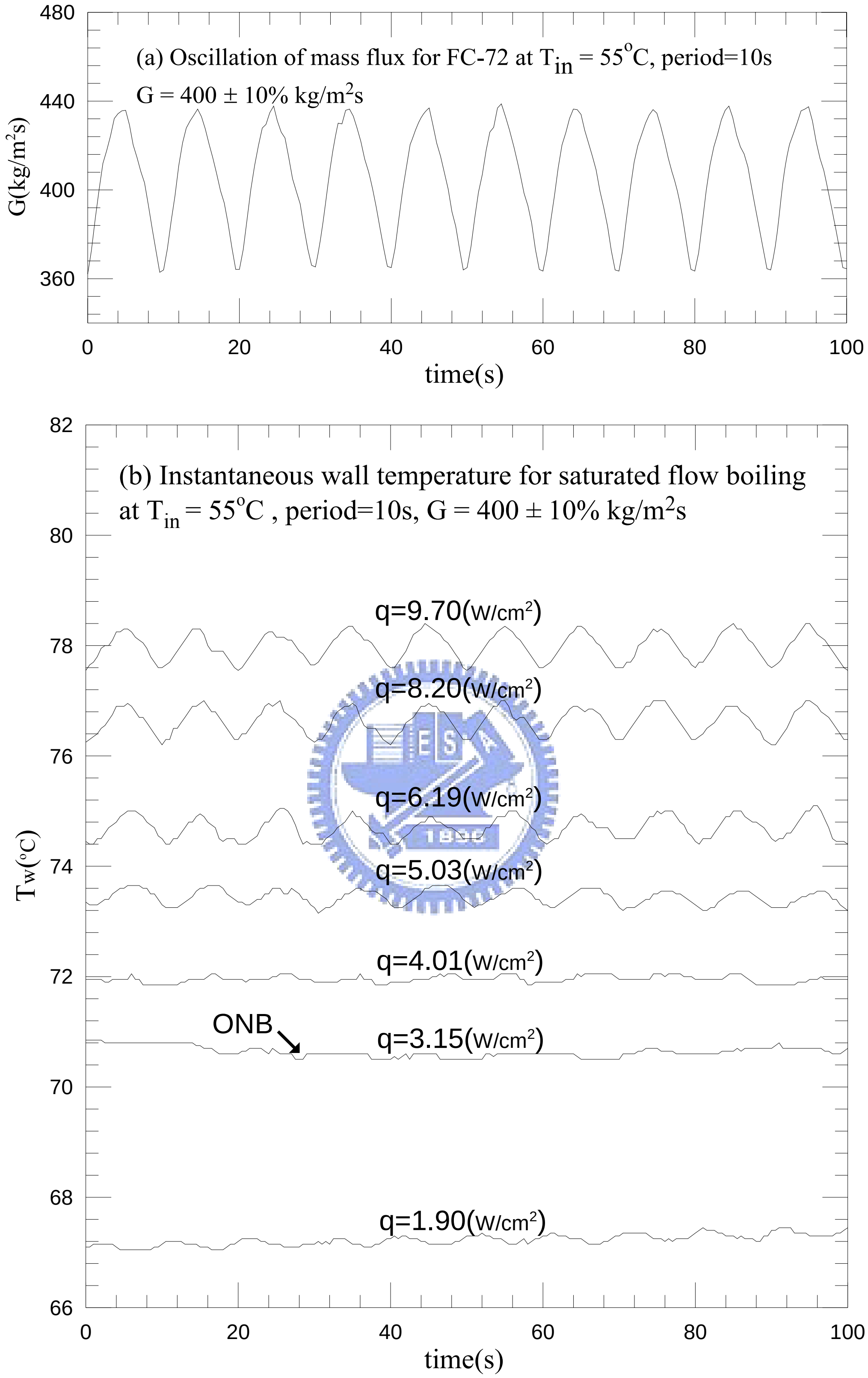

Fig. 4.14 Time variations of (a) imposed coolant mass flux and (b) copper plate temperature in transient oscillatory saturated flow boiling for various imposed heat fluxes for G=400±10% kg/m²s with t_p =10 sec.($\overline{q}_{ONB}$ =3.15 w/cm² at G =400 kg/m²s)

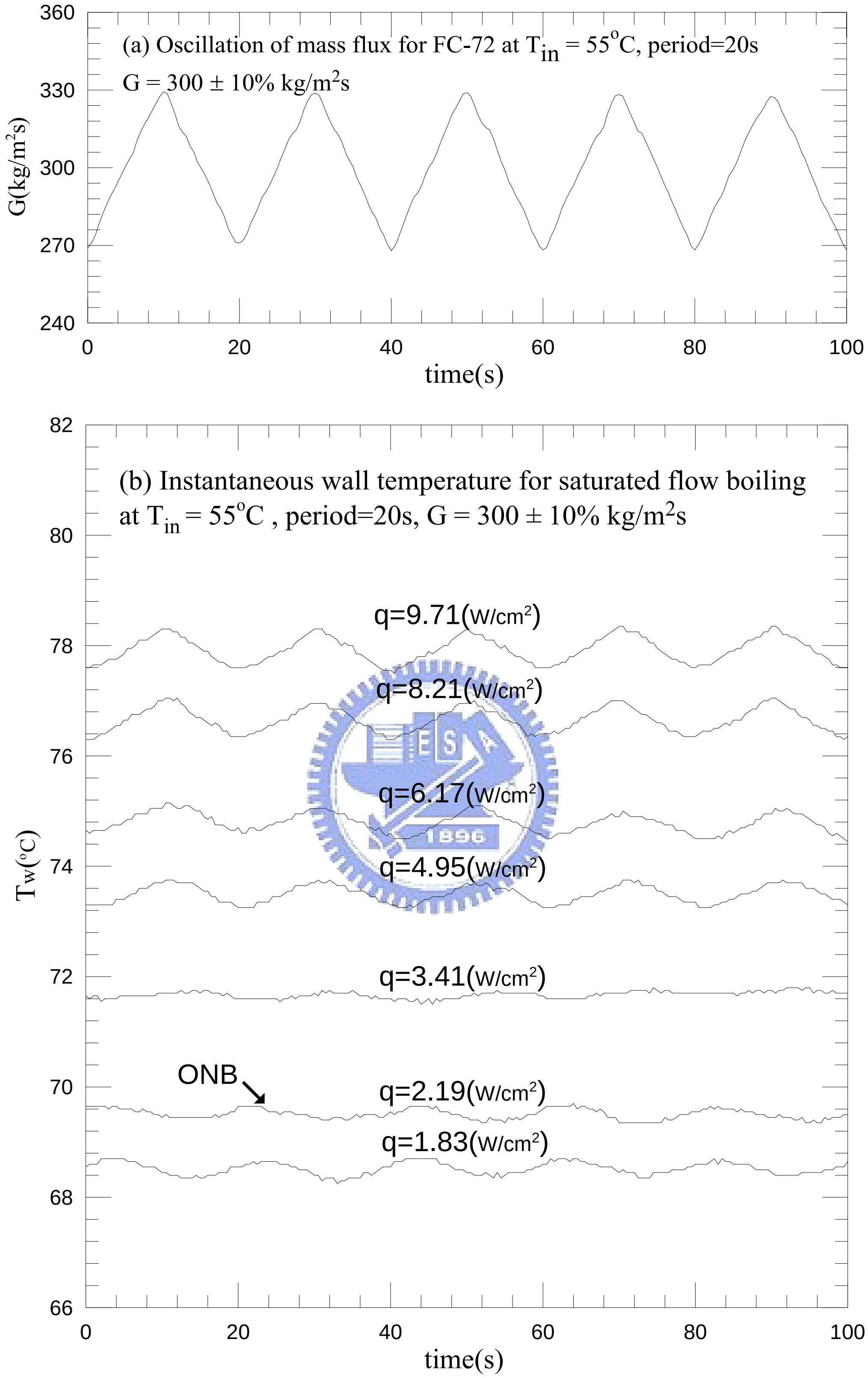

Fig. 4.15 Time variations of (a) imposed coolant mass flux and (b) copper plate temperature in transient oscillatory saturated flow boiling for various imposed heat fluxes for G=300±10% kg/m²s with t_p =20 sec.($\overline{q}_{ONB}$ =2.19 w/cm² at G =300 kg/m²s)

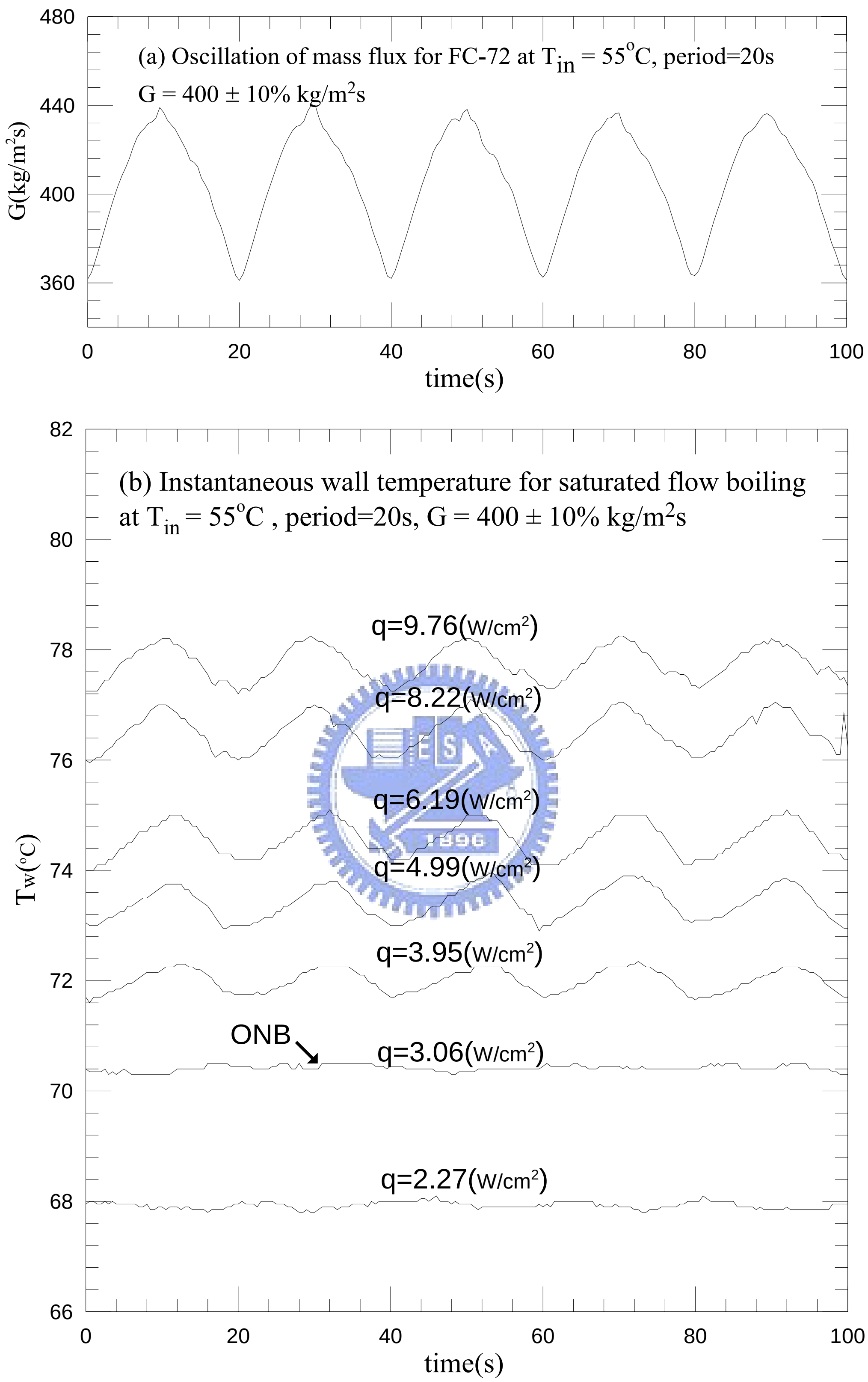

Fig. 4.16 Time variations of (a) imposed coolant mass flux and (b) copper plate temperature in transient oscillatory saturated flow boiling for various imposed heat fluxes for G=400±10% kg/m²s with t_p=20 sec.($\overline{q}_{ONB}$ =3.06 w/cm² at G =400 kg/m²s)

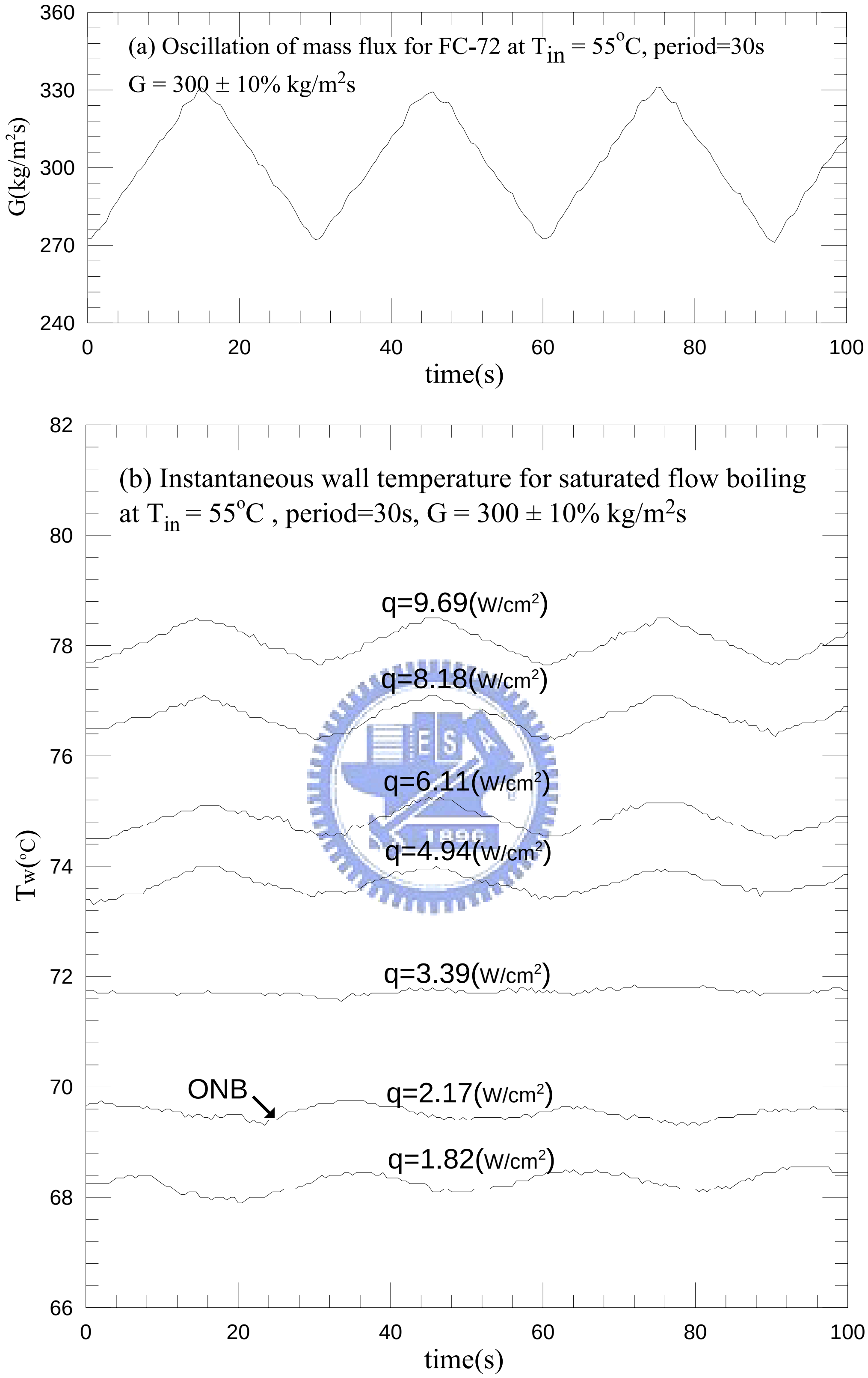

Fig. 4.17 Time variations of (a) imposed coolant mass flux and (b) copper plate temperature in transient oscillatory saturated flow boiling for various imposed heat fluxes for G=300±10% kg/m^{2}s with t_p=30 sec.($\overline{q}_{ONB}$=2.17 w/cm^2 at G =300 kg/m^{2}S)

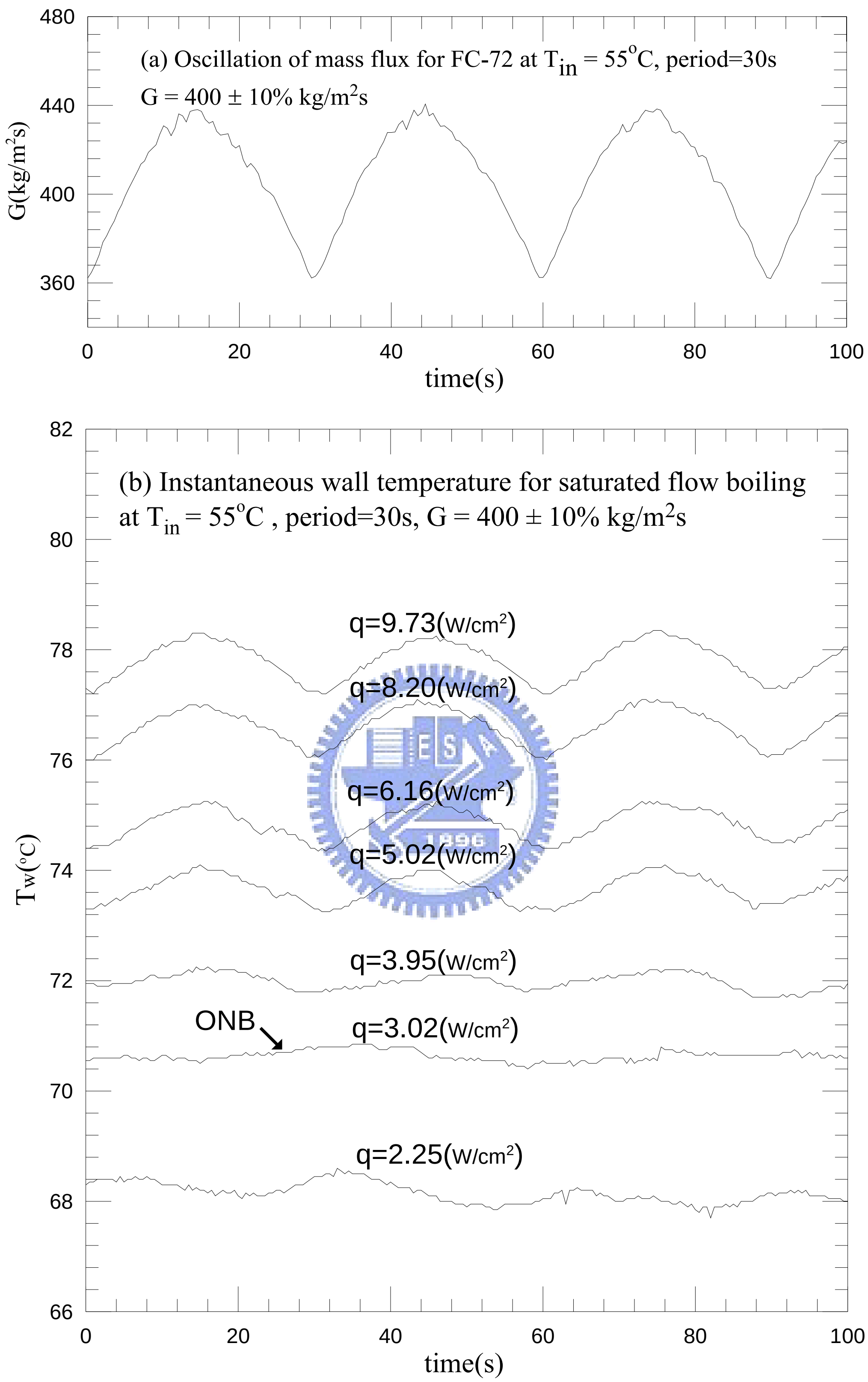

Fig. 4.18 Time variations of (a) imposed coolant mass flux and (b) copper plate temperature in transient oscillatory saturated flow boiling for various imposed heat fluxes for G=400±10% kg/m^{2}s with t_p=30 sec.($\overline{q}_{ONB}$ =3.02 w/cm^2 at G =400 kg/m^{2}S)

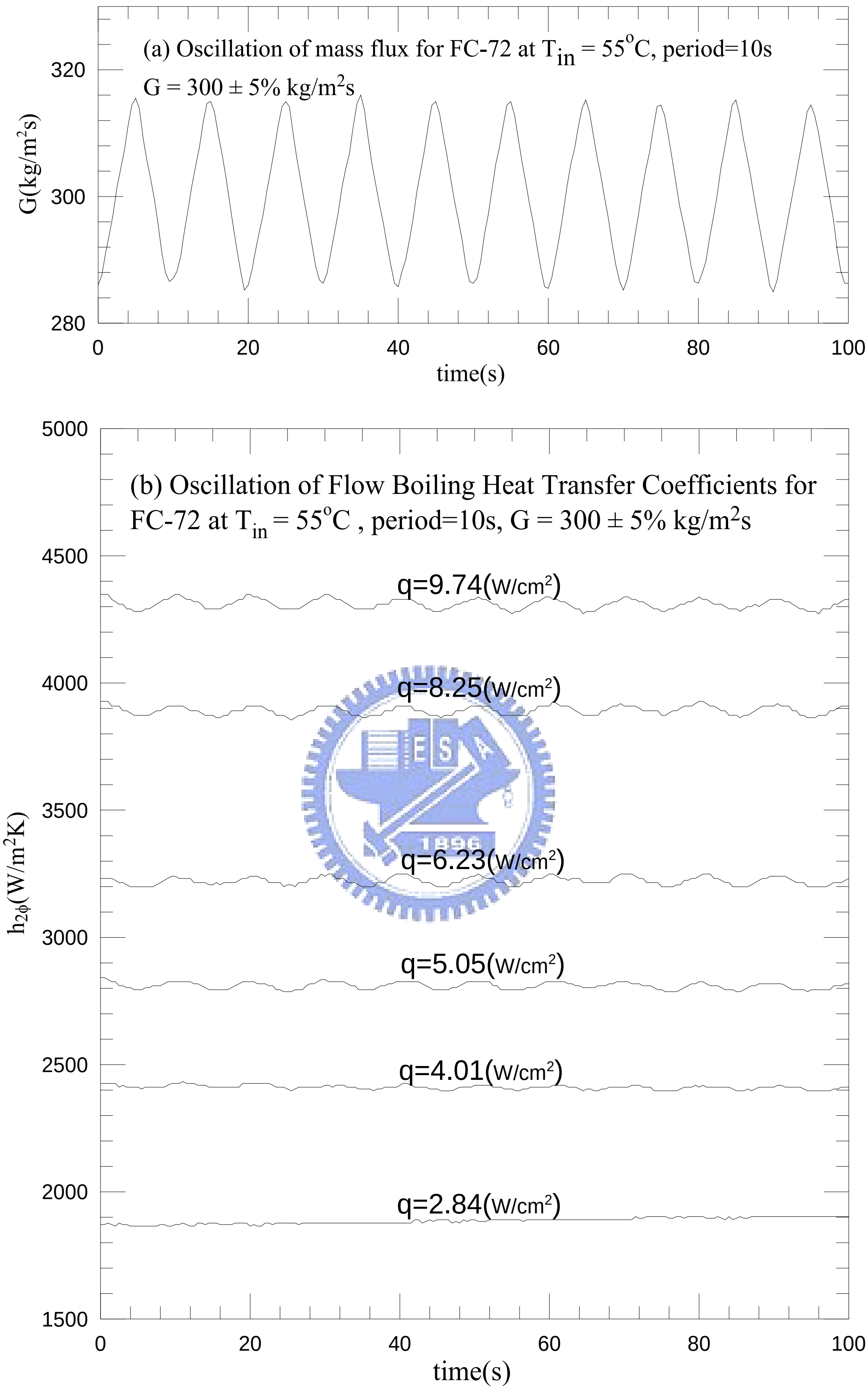

Fig. 4.19 Time variations of (a) imposed coolant mass flux and (b) flow boiling heat transfer coefficients in transient oscillatory saturated flow boiling for various imposed heat fluxes for G=300± 5% kg/m^{2}s with t_p=10 sec.

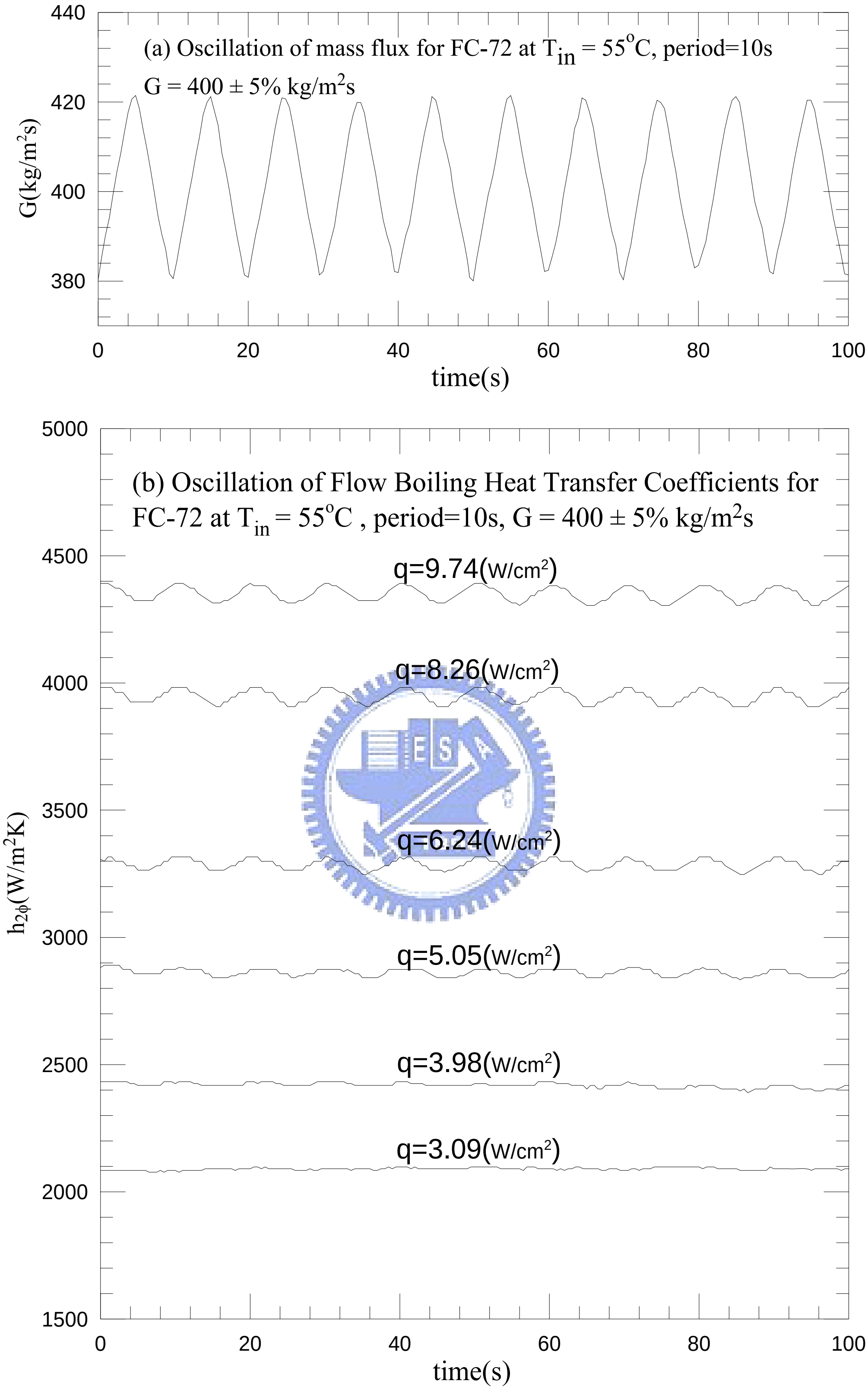

Fig. 4.20 Time variations of (a) imposed coolant mass flux and (b) flow boiling heat transfer coefficients in transient oscillatory saturated flow boiling for various imposed heat fluxes for G=400± 5% kg/m^{2}s with t_p=10 sec.

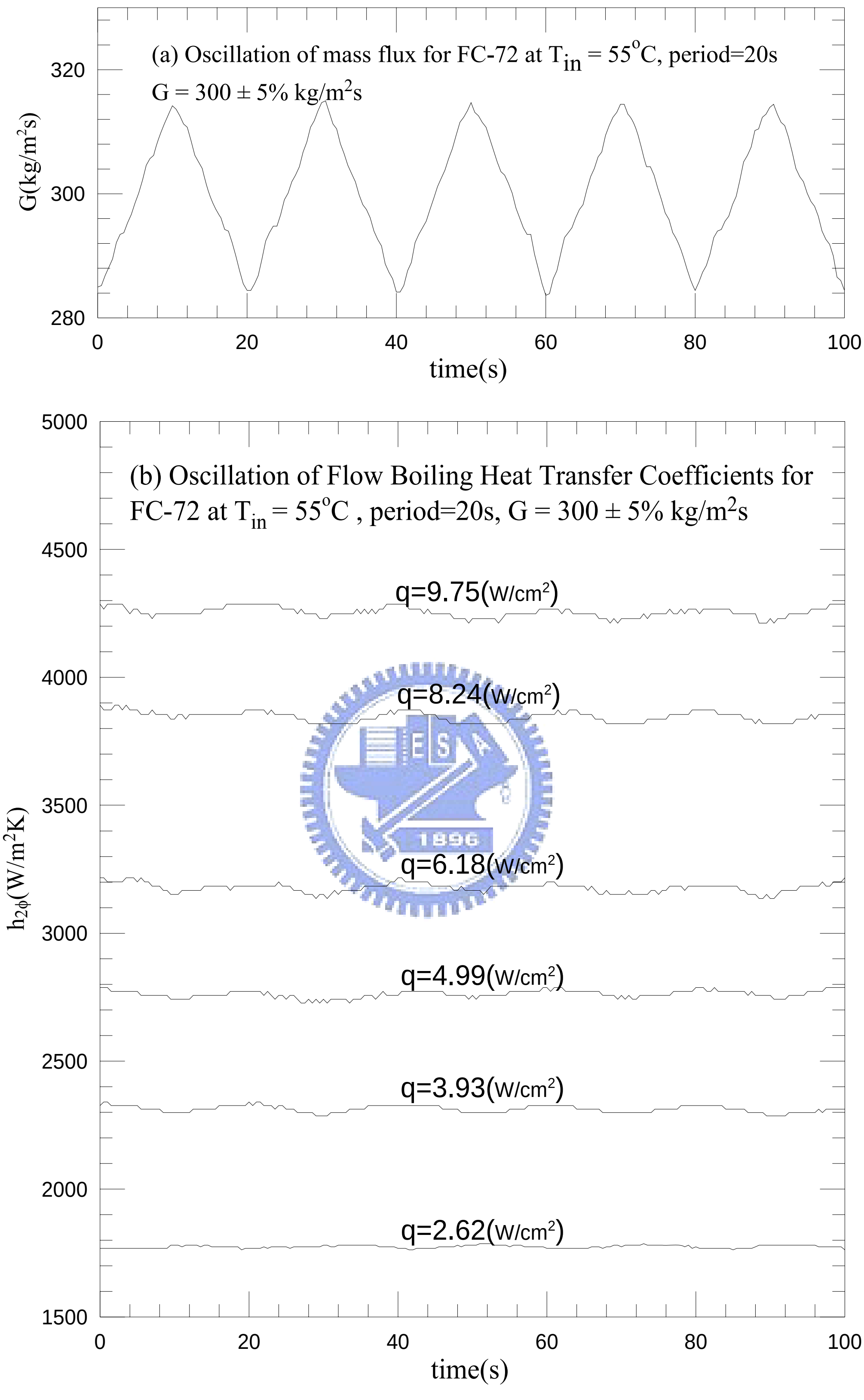

Fig. 4.21 Time variations of (a) imposed coolant mass flux and (b) flow boiling heat transfer coefficients in transient oscillatory saturated flow boiling for various imposed heat fluxes for G=300± 5% kg/m^{2}s with t_p=20 sec.

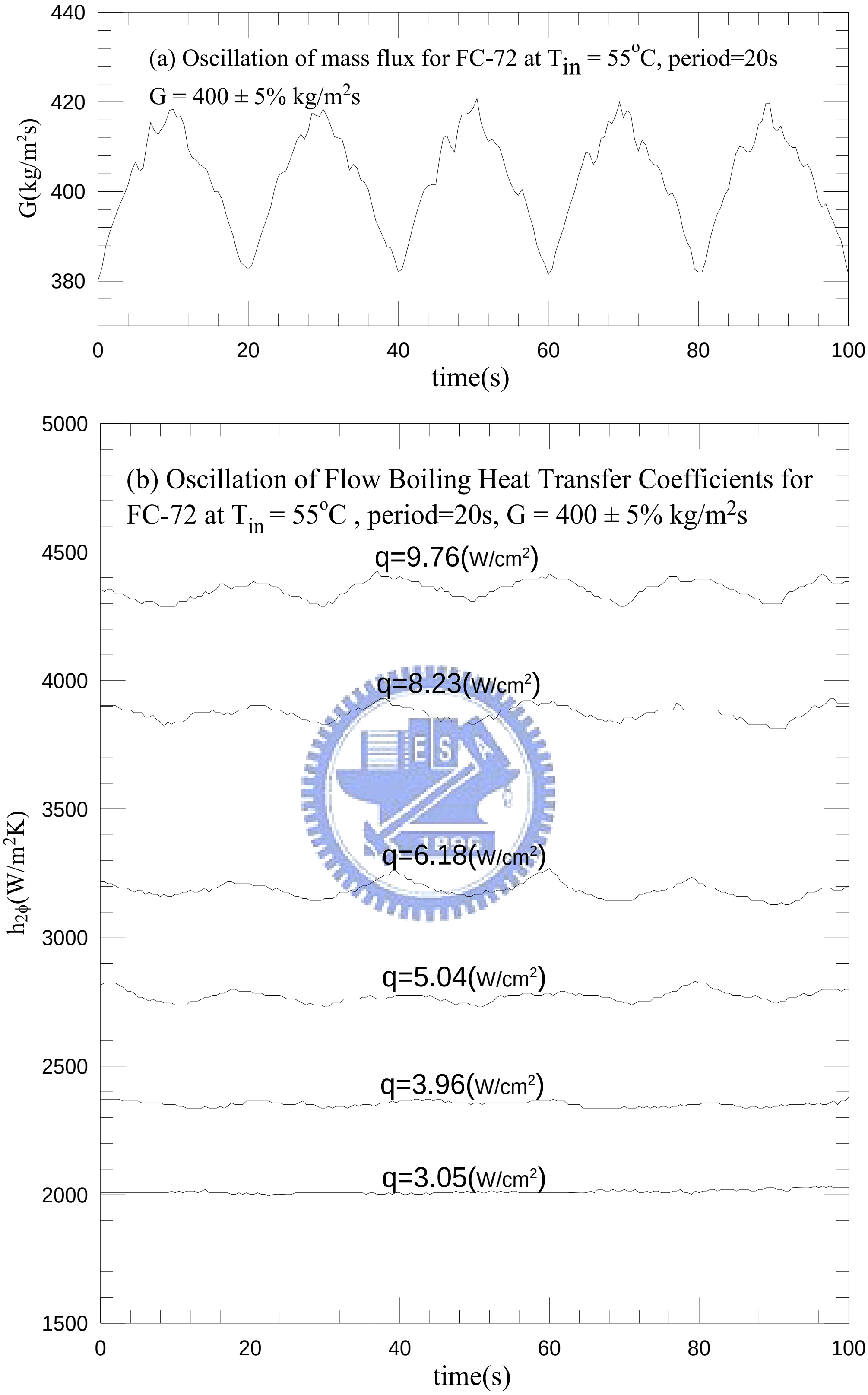

Fig. 4.22 Time variations of (a) imposed coolant mass flux and (b) flow boiling heat transfer coefficients in transient oscillatory saturated flow boiling for various imposed heat fluxes for G=400± 5% kg/m^{2}s with t_p=20 sec.

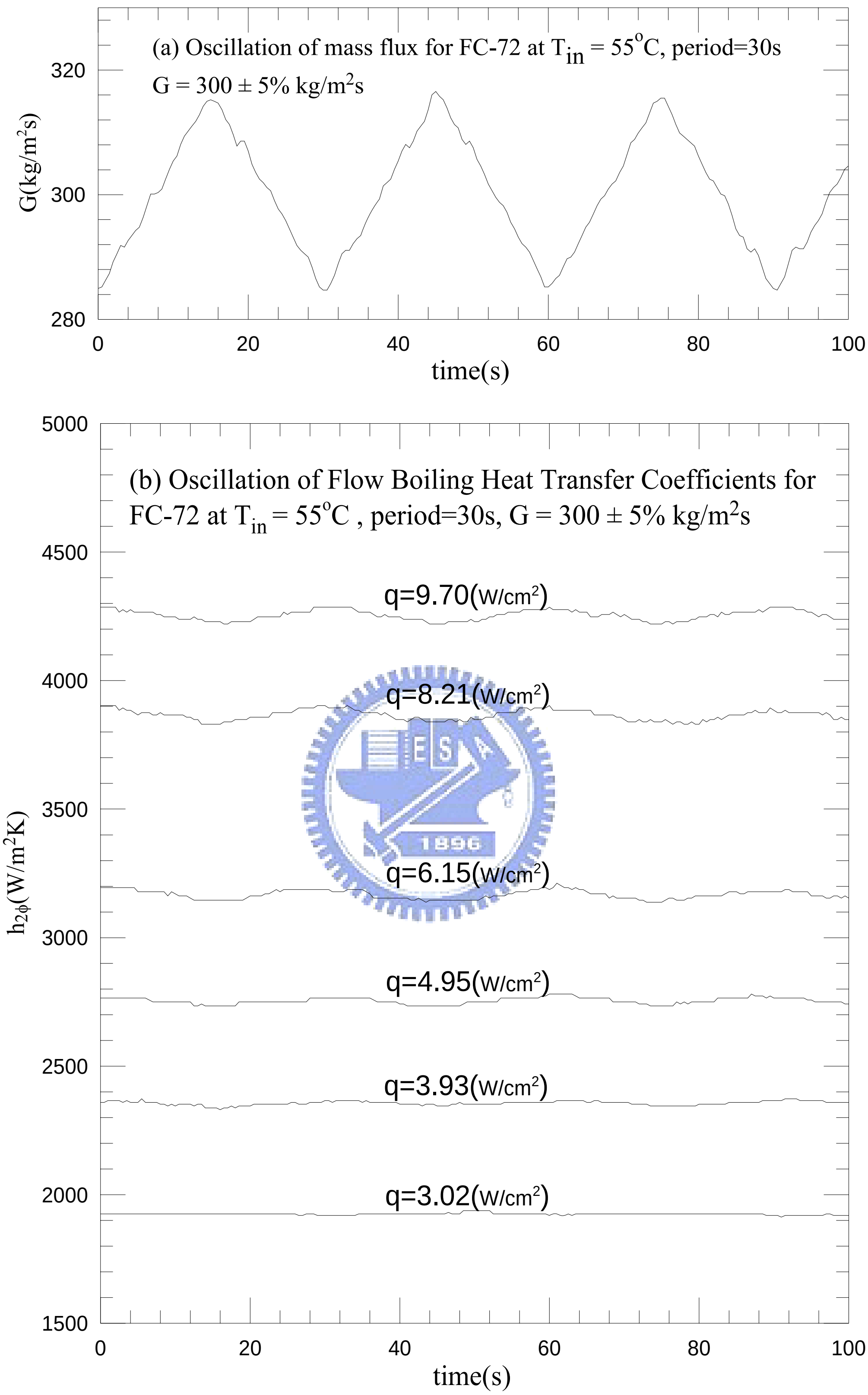

Fig. 4.23 Time variations of (a) imposed coolant mass flux and (b) flow boiling heat transfer coefficients in transient oscillatory saturated flow boiling for various imposed heat fluxes for G=300± 5% kg/m^{2}s with t_p=30 sec.

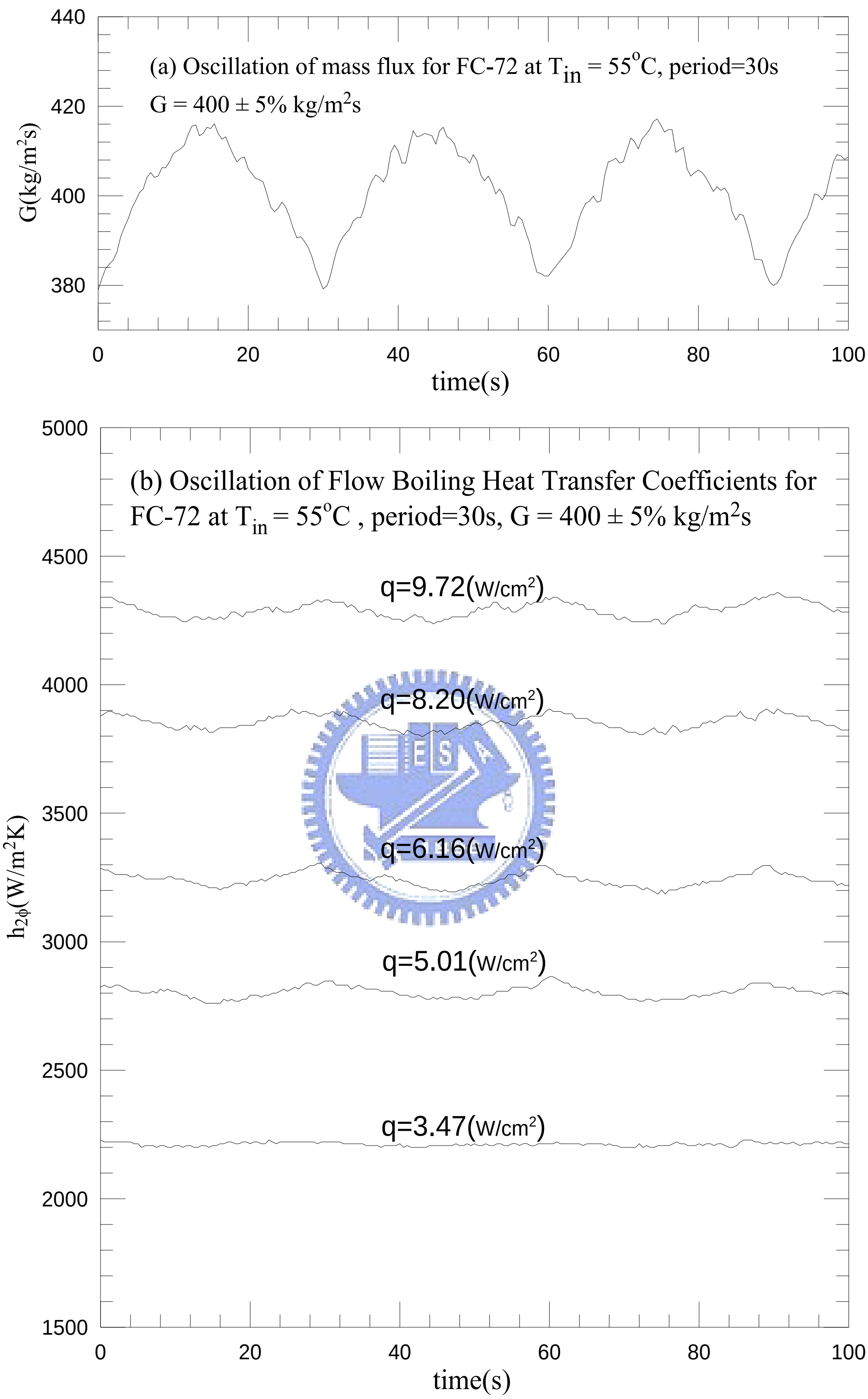

Fig. 4.24 Time variations of (a) imposed coolant mass flux and (b) flow boiling heat transfer coefficients in transient oscillatory saturated flow boiling for various imposed heat fluxes for G=400± 5% kg/m^{2}s with t_p=30 sec.

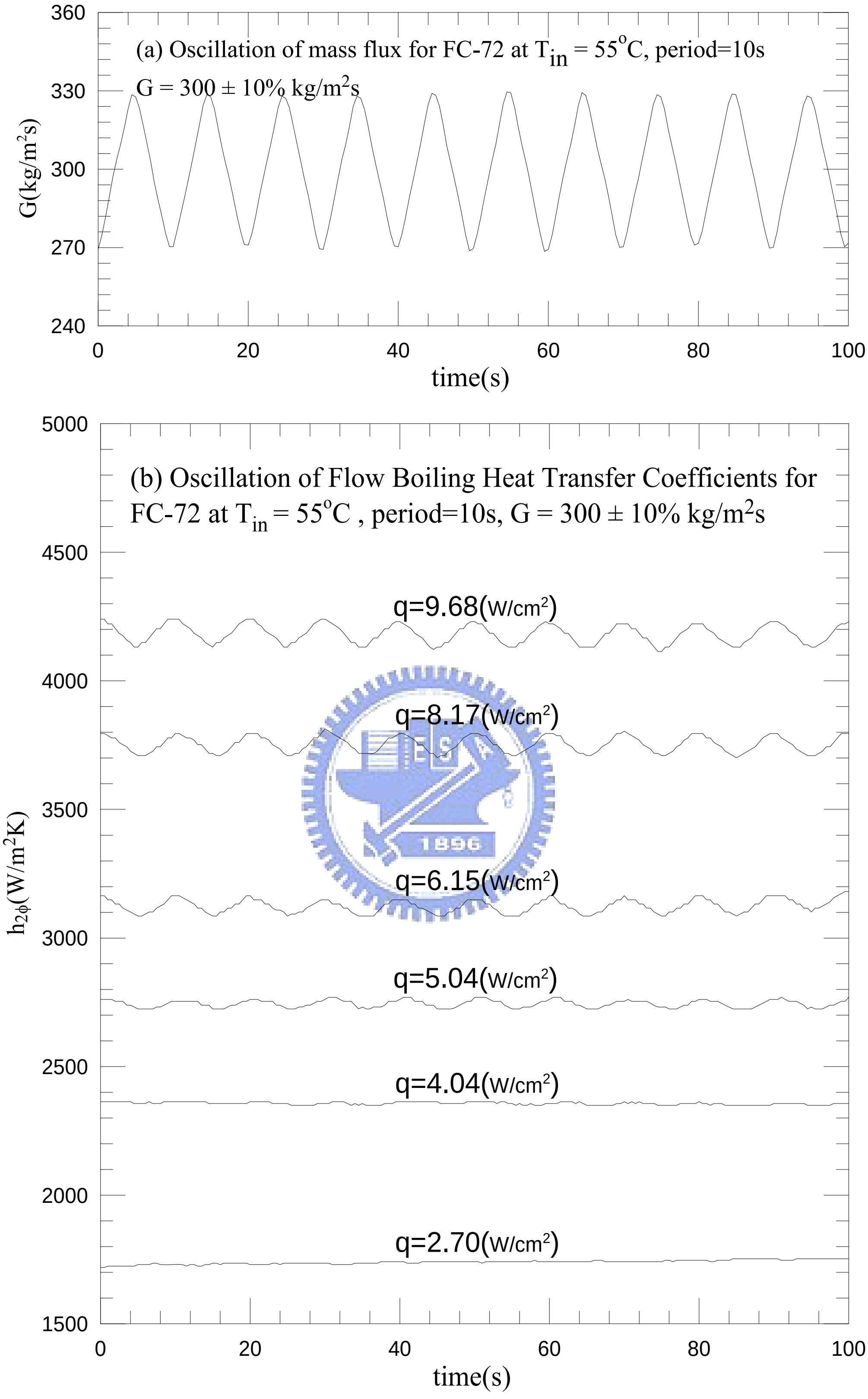

Fig. 4.25 Time variations of (a) imposed coolant mass flux and (b) flow boiling heat transfer coefficients in transient oscillatory saturated flow boiling for various imposed heat fluxes for G=300± 10% kg/m^{2}s with t_p=10 sec.

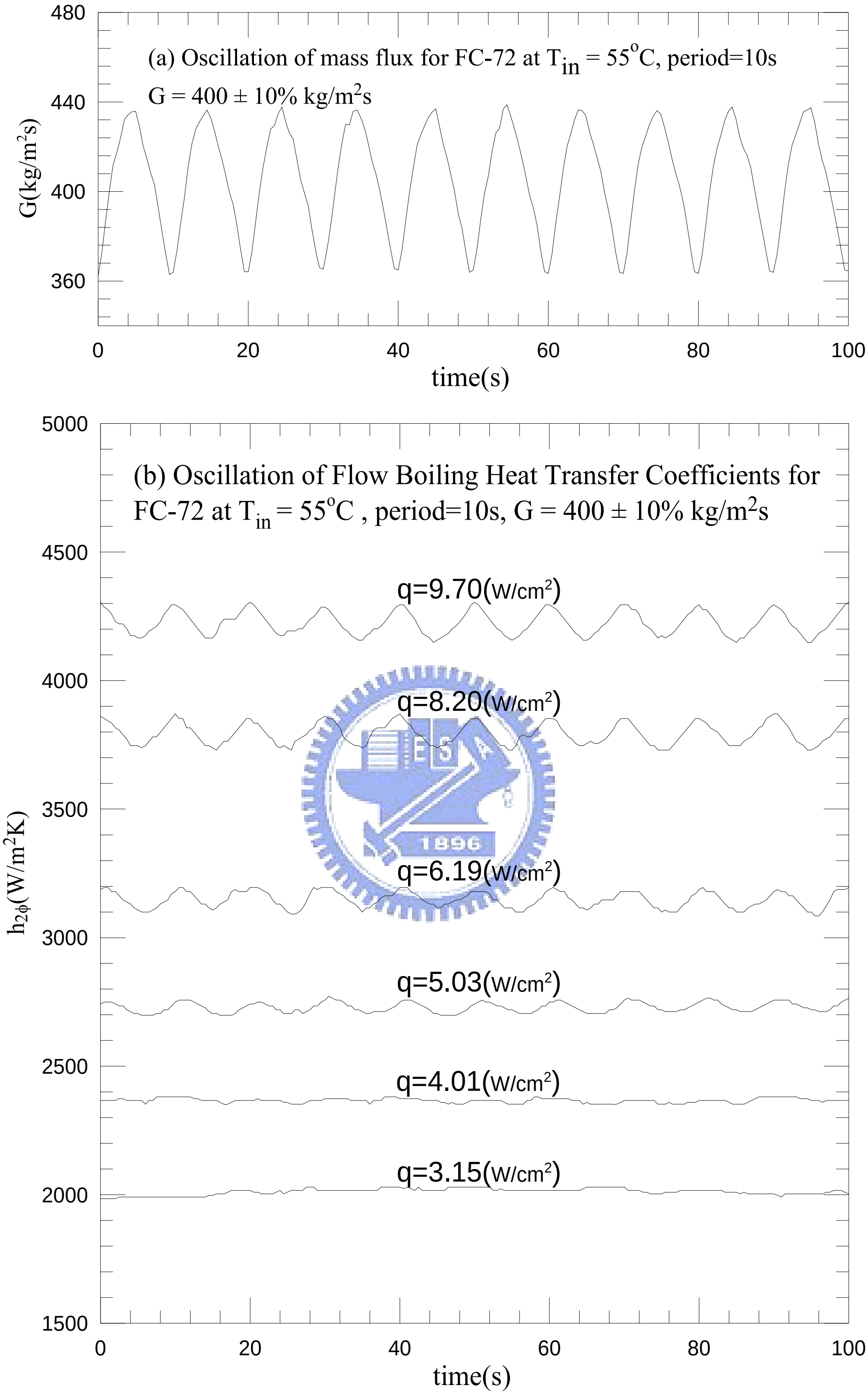

Fig. 4.26 Time variations of (a) imposed coolant mass flux and (b) flow boiling heat transfer coefficients in transient oscillatory saturated flow boiling for various imposed heat fluxes for G=400± 10% kg/m^{2}s with t_p=10 sec.

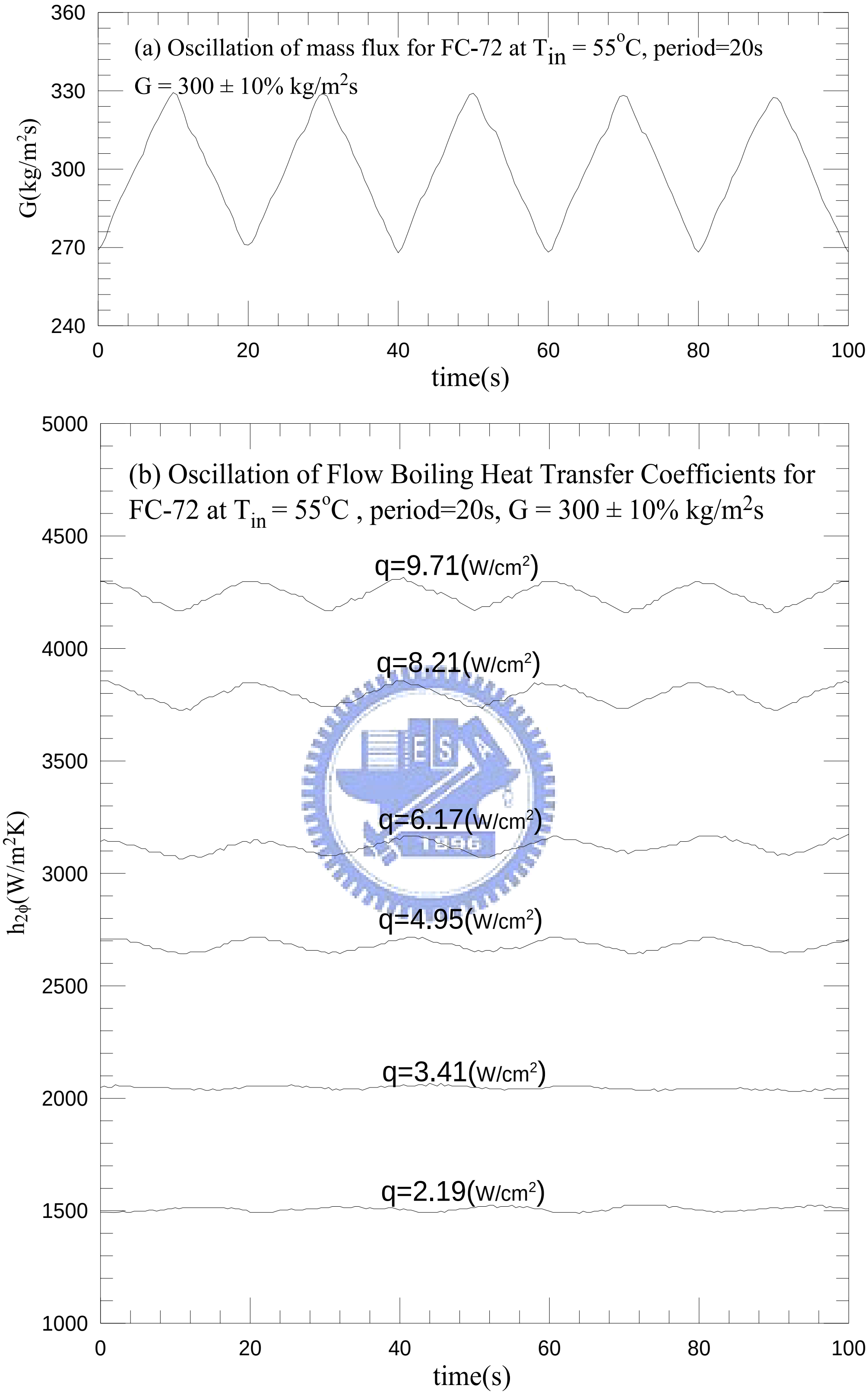

Fig. 4.27 Time variations of (a) imposed coolant mass flux and (b) flow boiling heat transfer coefficients in transient oscillatory saturated flow boiling for various imposed heat fluxes for G=300± 10% kg/m^{2}s with t_p=20 sec.

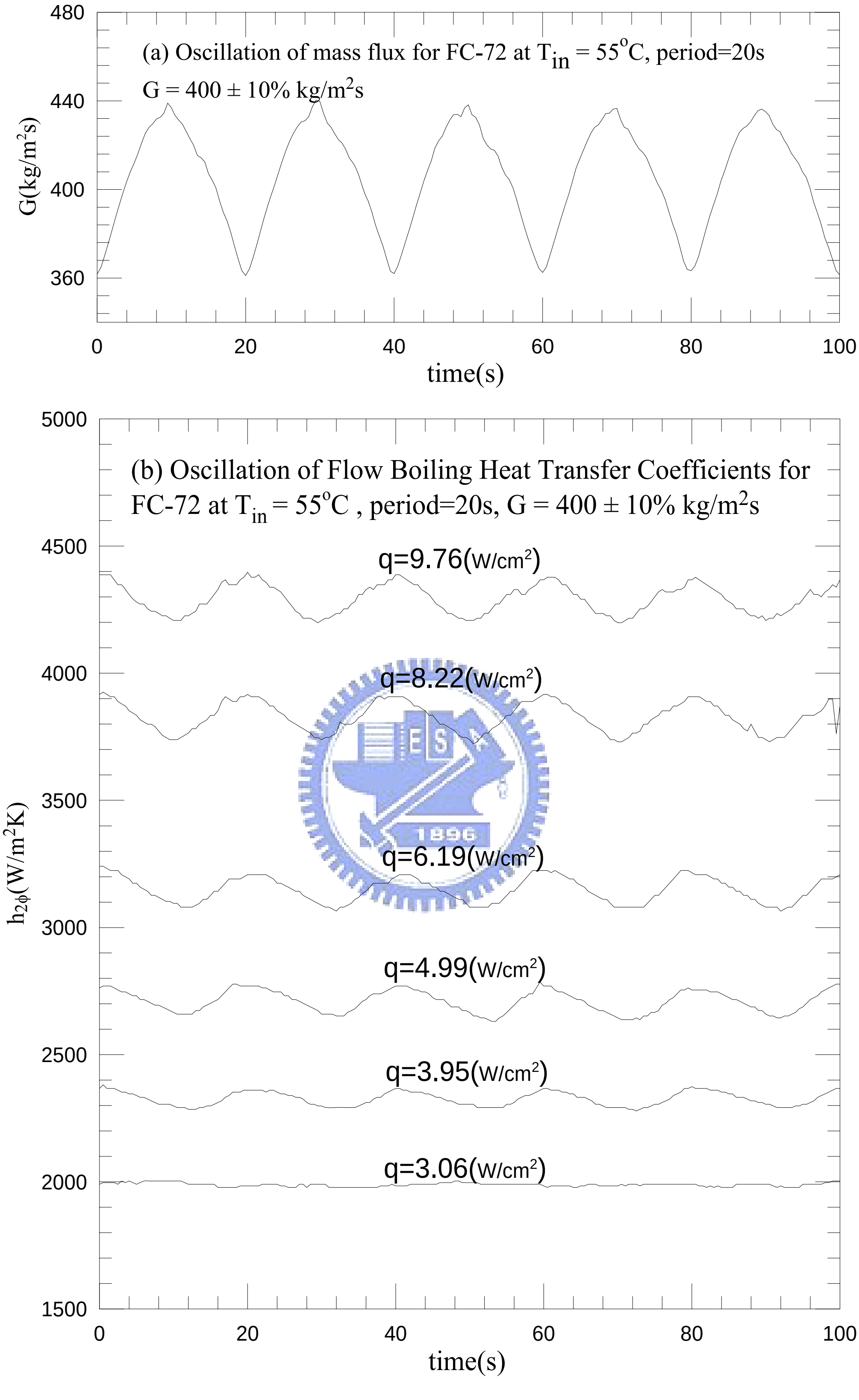

Fig. 4.28 Time variations of (a) imposed coolant mass flux and (b) flow boiling heat transfer coefficients in transient oscillatory saturated flow boiling for various imposed heat fluxes for G=400± 10% kg/m²s with t_p =20 sec.

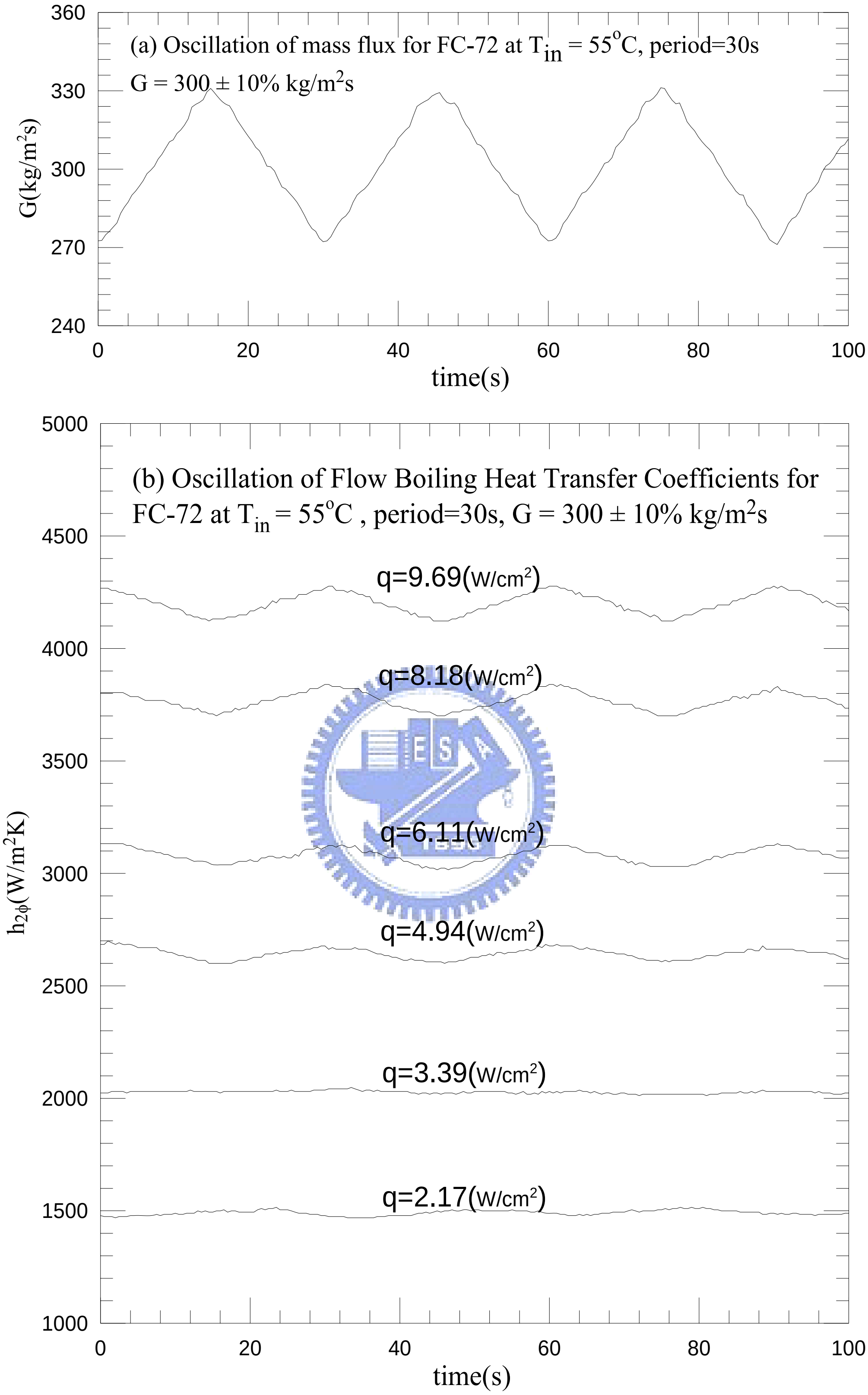

Fig. 4.29 Time variations of (a) imposed coolant mass flux and (b) flow boiling heat transfer coefficients in transient oscillatory saturated flow boiling for various imposed heat fluxes for G=300± 10% kg/m^{2}s with t_p=30 sec.

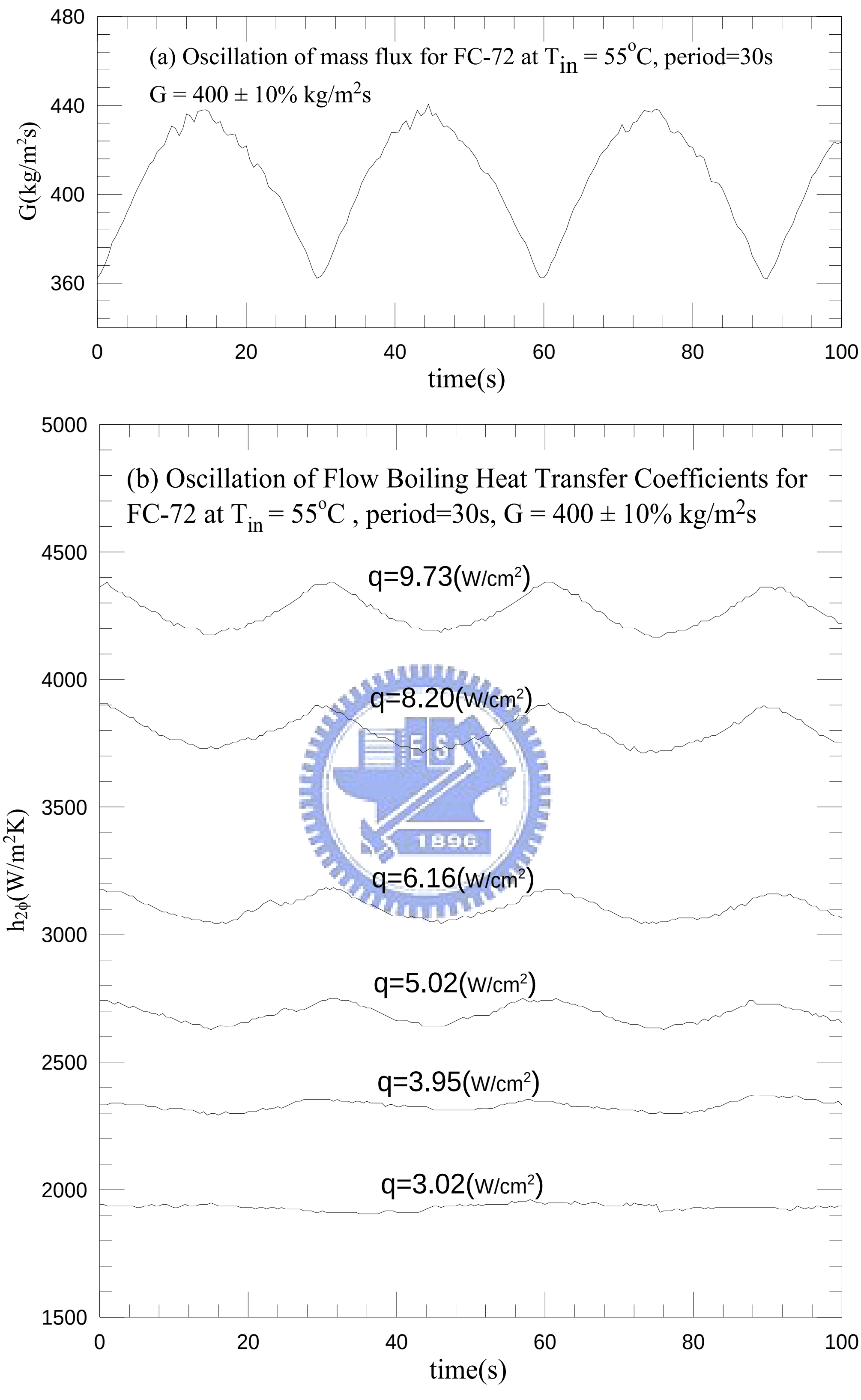

Fig. 4.30 Time variations of (a) imposed coolant mass flux and (b) flow boiling heat transfer coefficients in transient oscillatory saturated flow boiling for various imposed heat fluxes for G=400± 10% kg/m²s with t_p=30 sec.

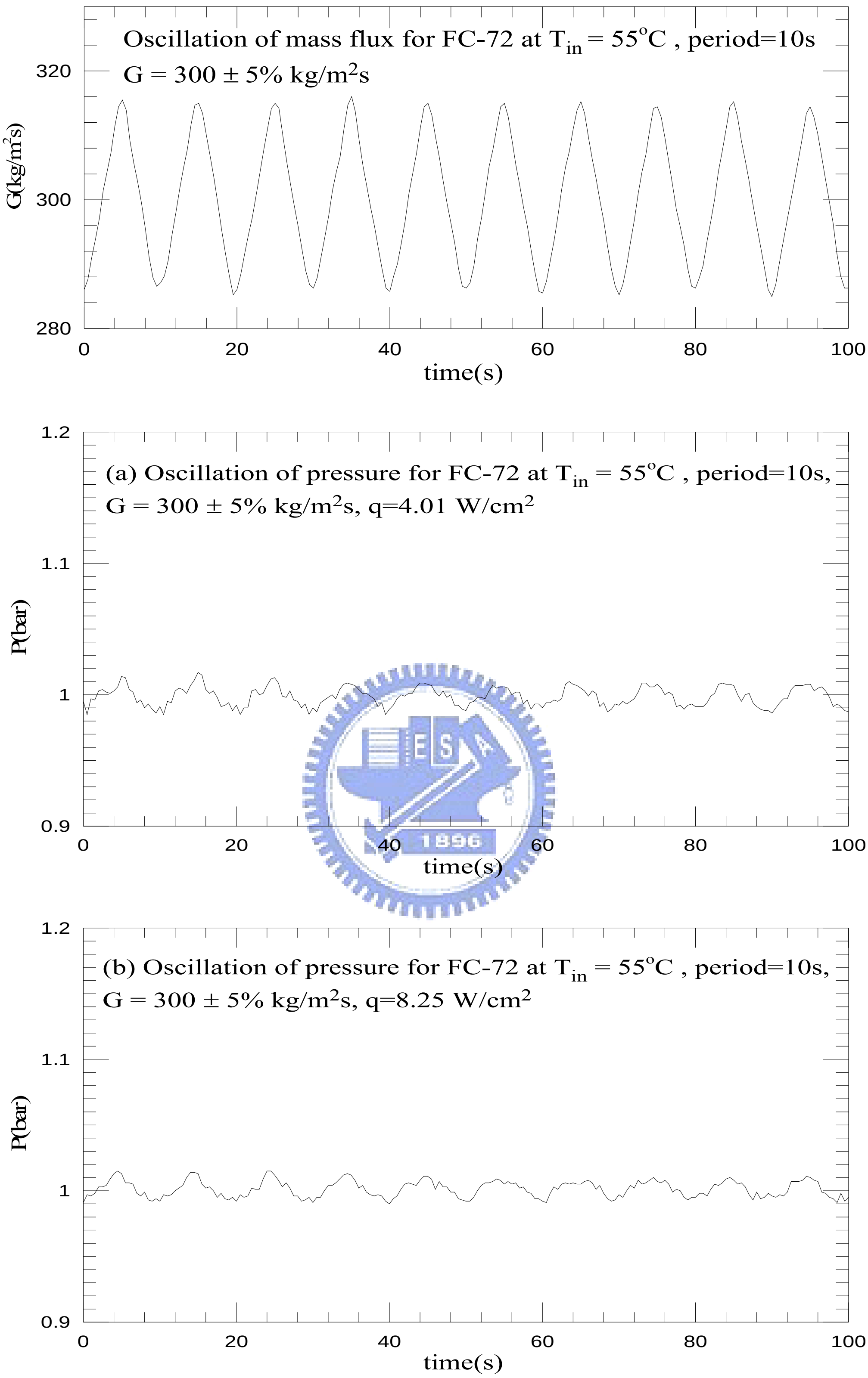

Fig.4.31 Time variations of coolant mass flux and inlet pressure in transient oscillatory saturated flow boiling for various imposed heat fluxes at (a) q=4.01 W/cm^2 and (b) q=8.25 W/cm^2 for G=300±5% kg/m^2s with t_p=10 sec.

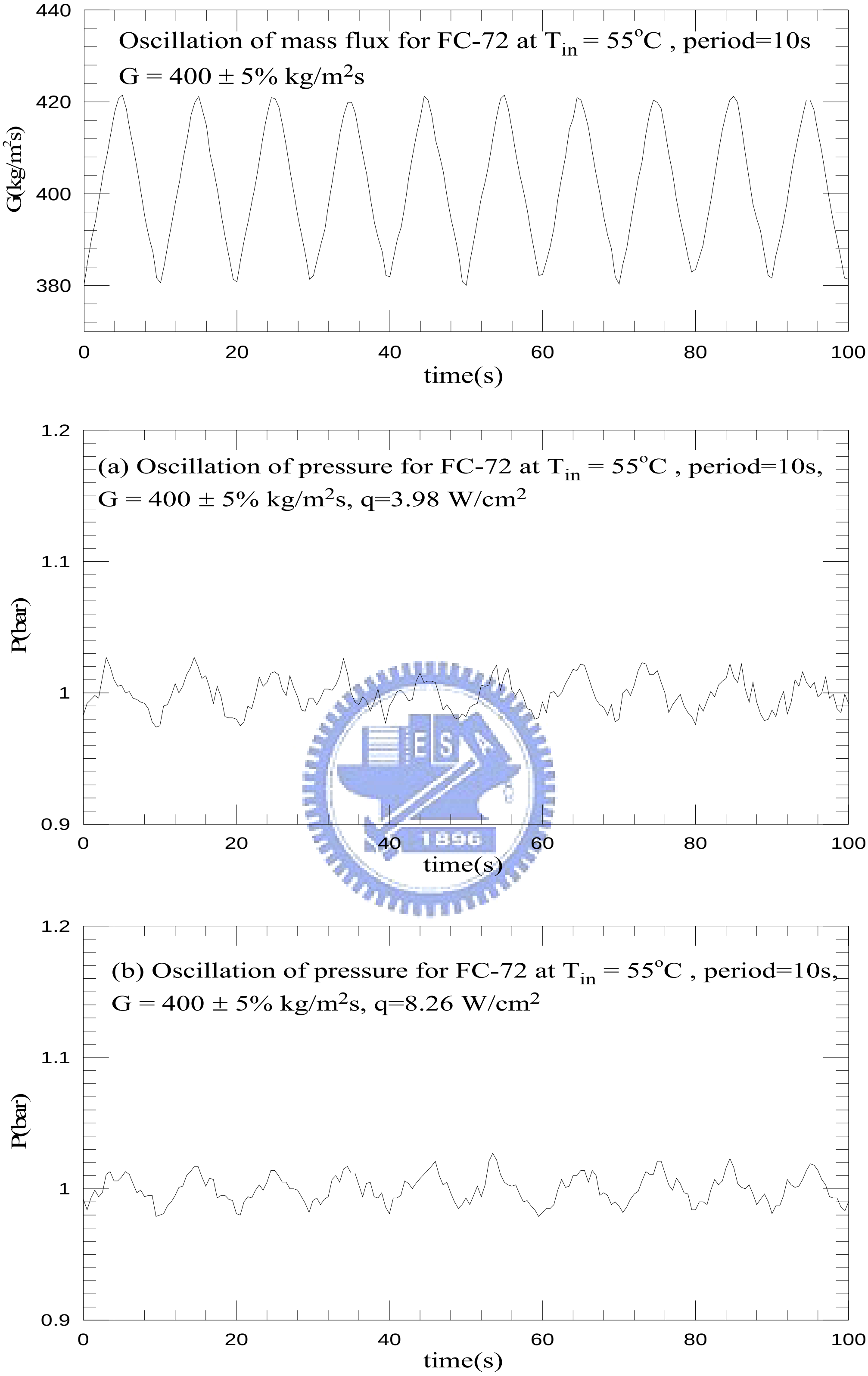

Fig.4.32 Time variations of coolant mass flux and inlet pressure in transient oscillatory saturated flow boiling for various imposed heat fluxes at (a) $q=3.98\ W/cm^2$ and (b) $q=8.26\ W/cm^2$ for $G=400\pm5\%\ kg/m^2s$ with $t_p=10$ sec.

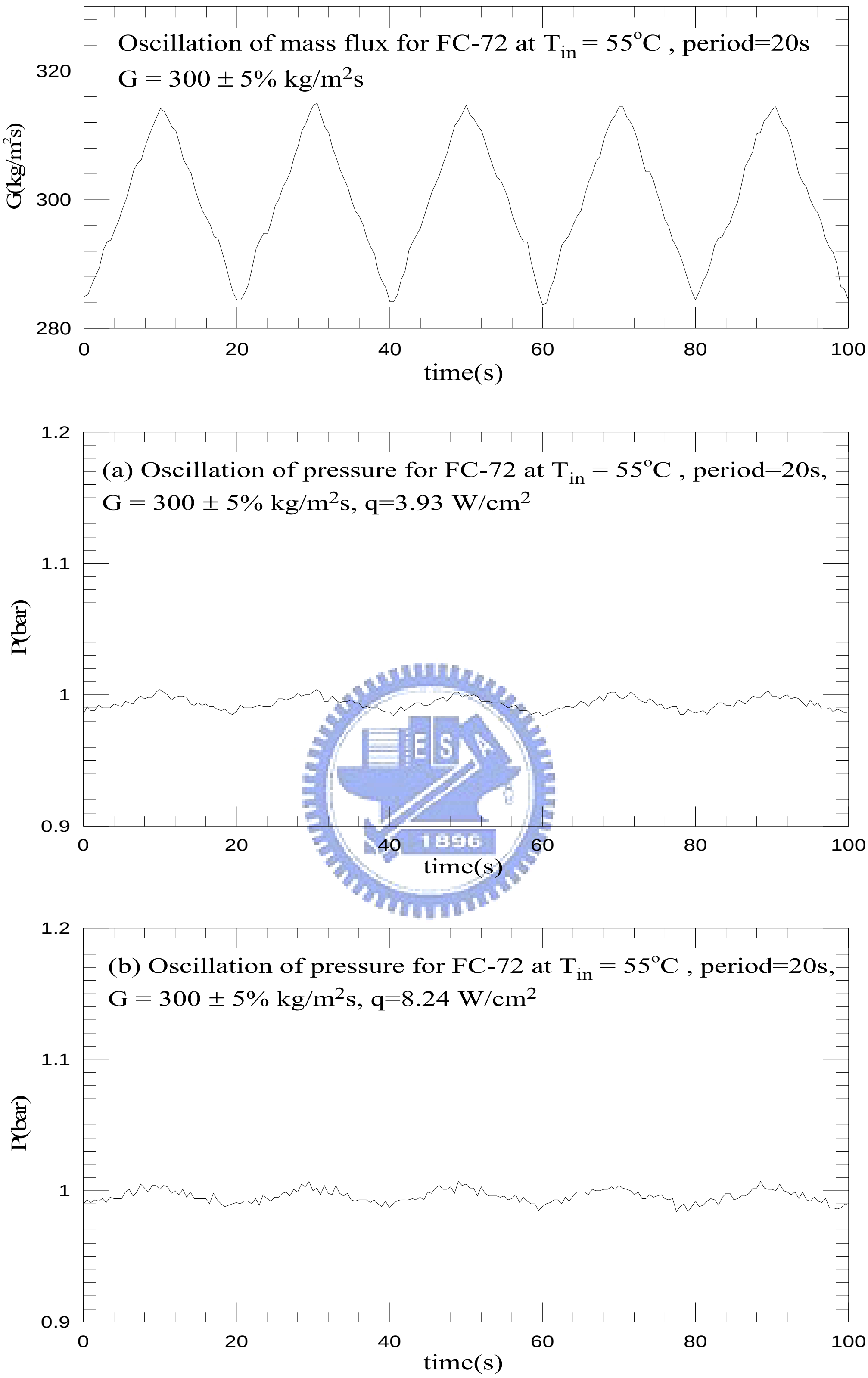

Fig.4.33 Time variations of coolant mass flux and inlet pressure in transient oscillatory saturated flow boiling for various imposed heat fluxes at (a) q=3.93 W/cm^2 and (b) q=8.24 W/cm^2 for G=300±5% kg/m^{2}s with t_p=20 sec.

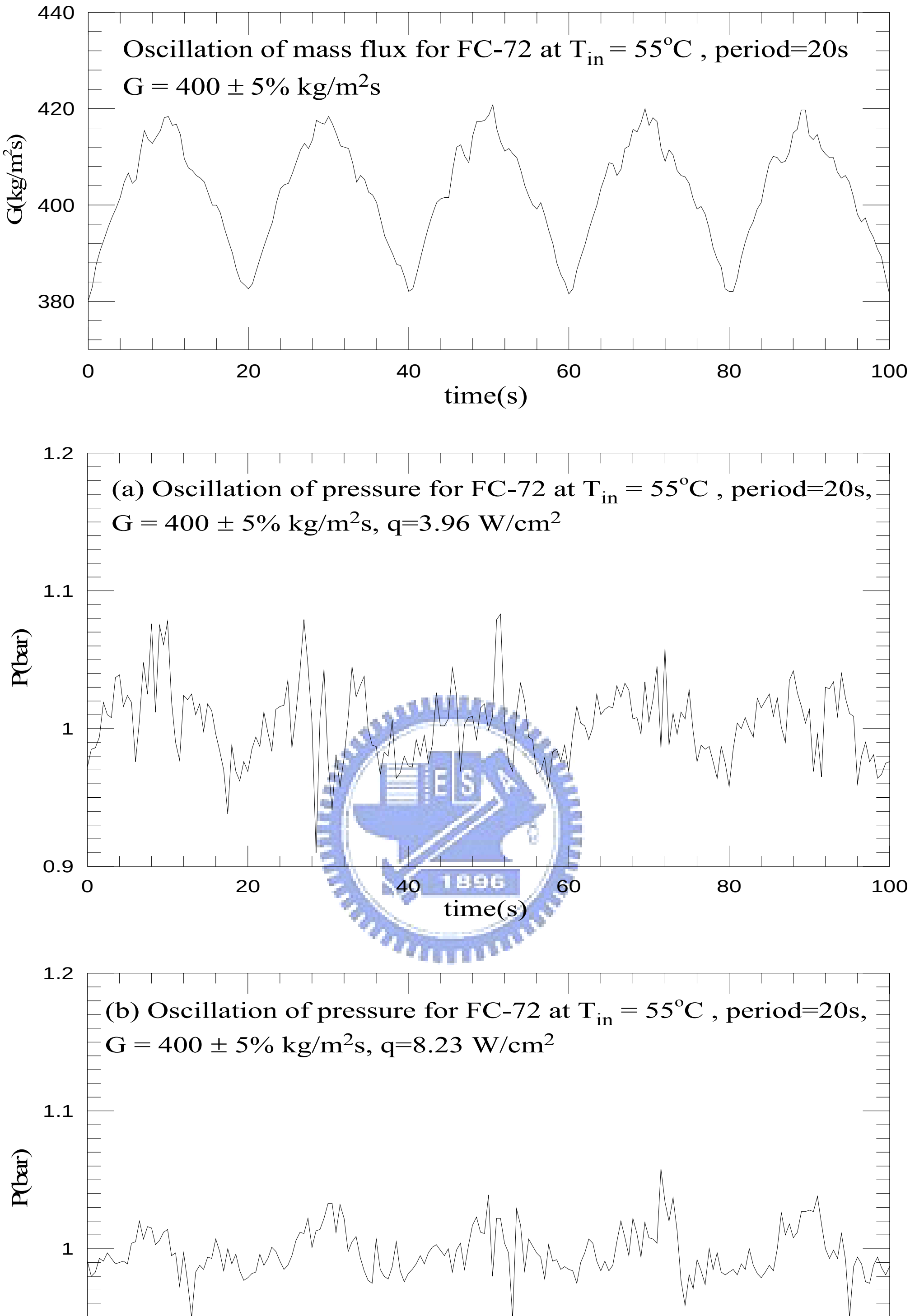

Fig.4.34 Time variations of coolant mass flux and inlet pressure in transient oscillatory saturated flow boiling for various imposed heat fluxes at (a) q=3.96 W/cm^2 and (b) q=8.23 W/cm^2 for G=400±5% kg/m^{2}s with t_p=20 sec.

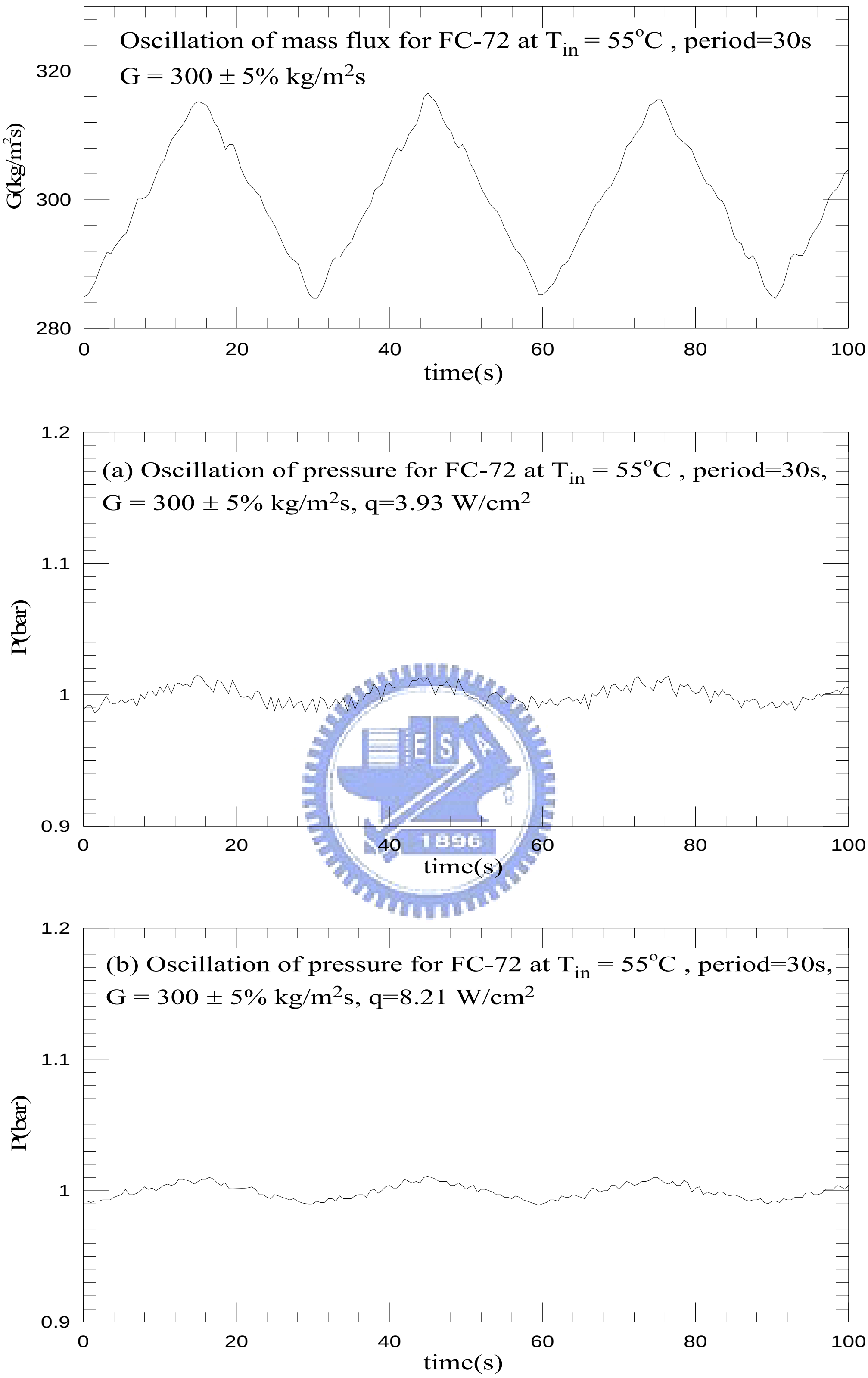

Fig.4.35 Time variations of coolant mass flux and inlet pressure in transient oscillatory saturated flow boiling for various imposed heat fluxes at (a) q=3.93 W/cm^2 and (b) q=8.21 W/cm^2 for G=300±5% kg/m^{2}s with t_p=30 sec.

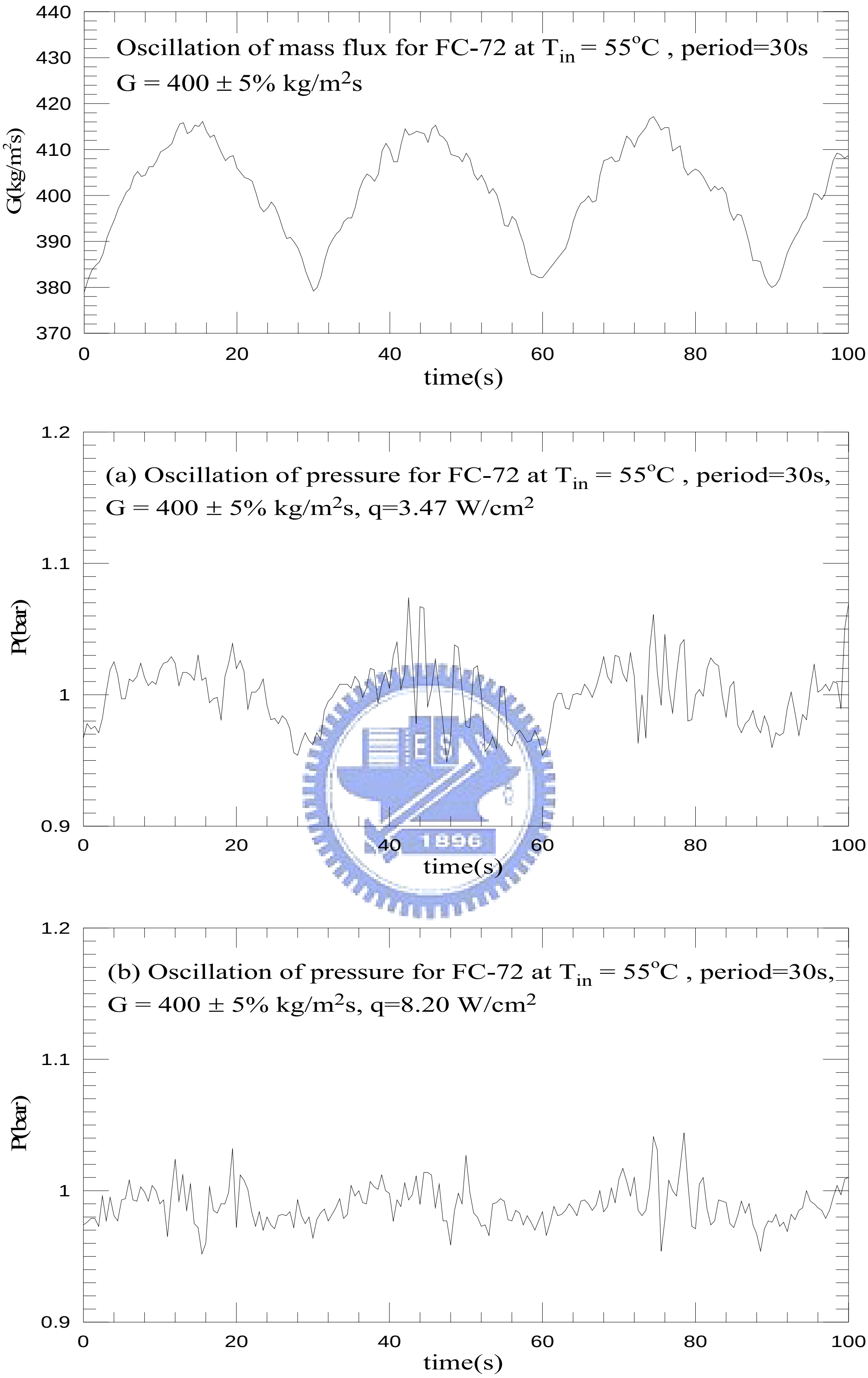

Fig.4.36 Time variations of coolant mass flux and inlet pressure in transient oscillatory saturated flow boiling for various imposed heat fluxes at (a) q=3.47 W/cm^2 and (b) q=8.20 W/cm^2 for G=400±5% kg/m^{2}s with t_p=30 sec.

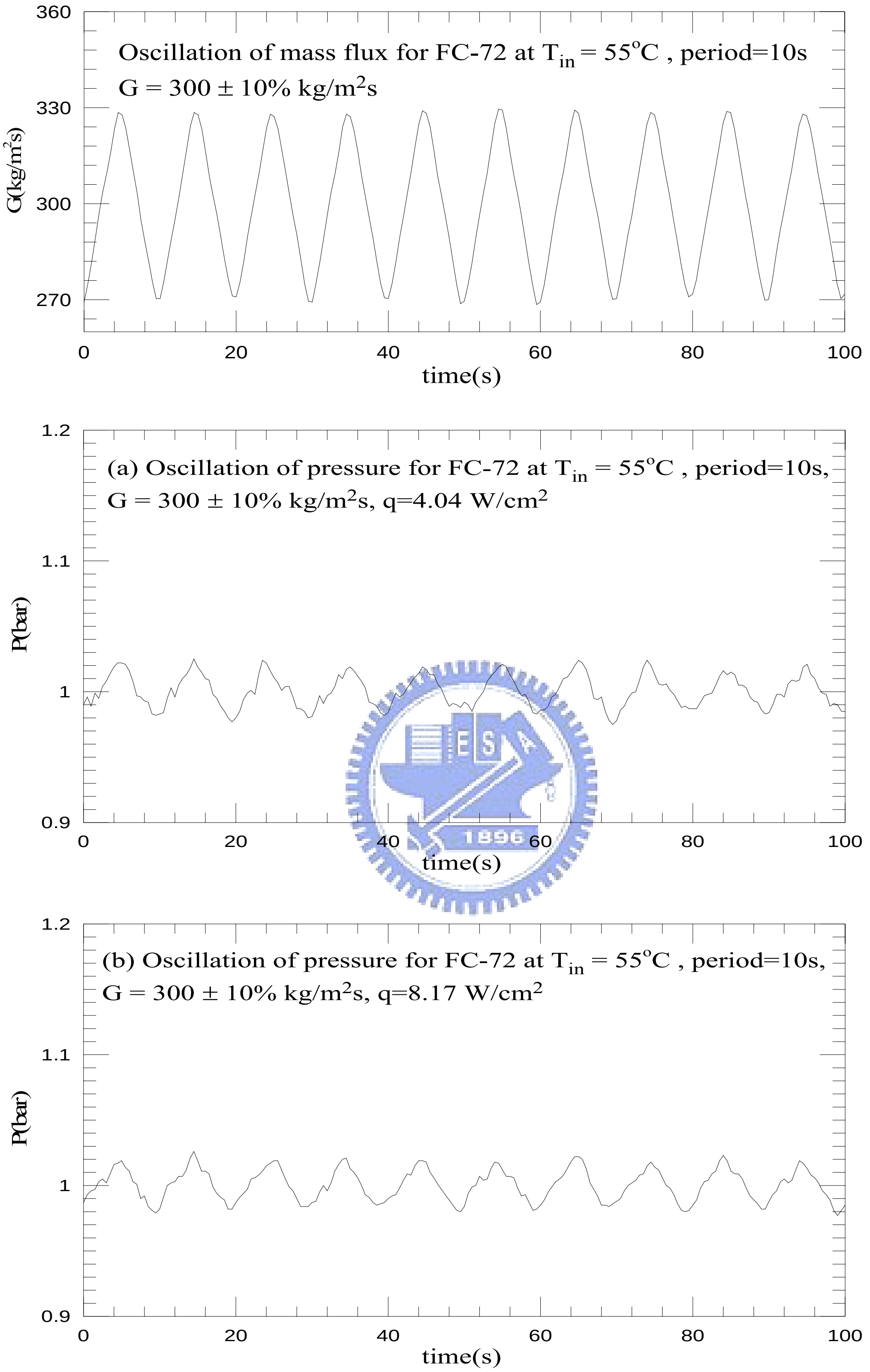

Fig.4.37 Time variations of coolant mass flux and inlet pressure in transient oscillatory saturated flow boiling for various imposed heat fluxes at (a) q=4.04 W/cm^2 and (b) q=8.17 W/cm^2 for G=300±10% kg/m^{2}s with t_p=10 sec.

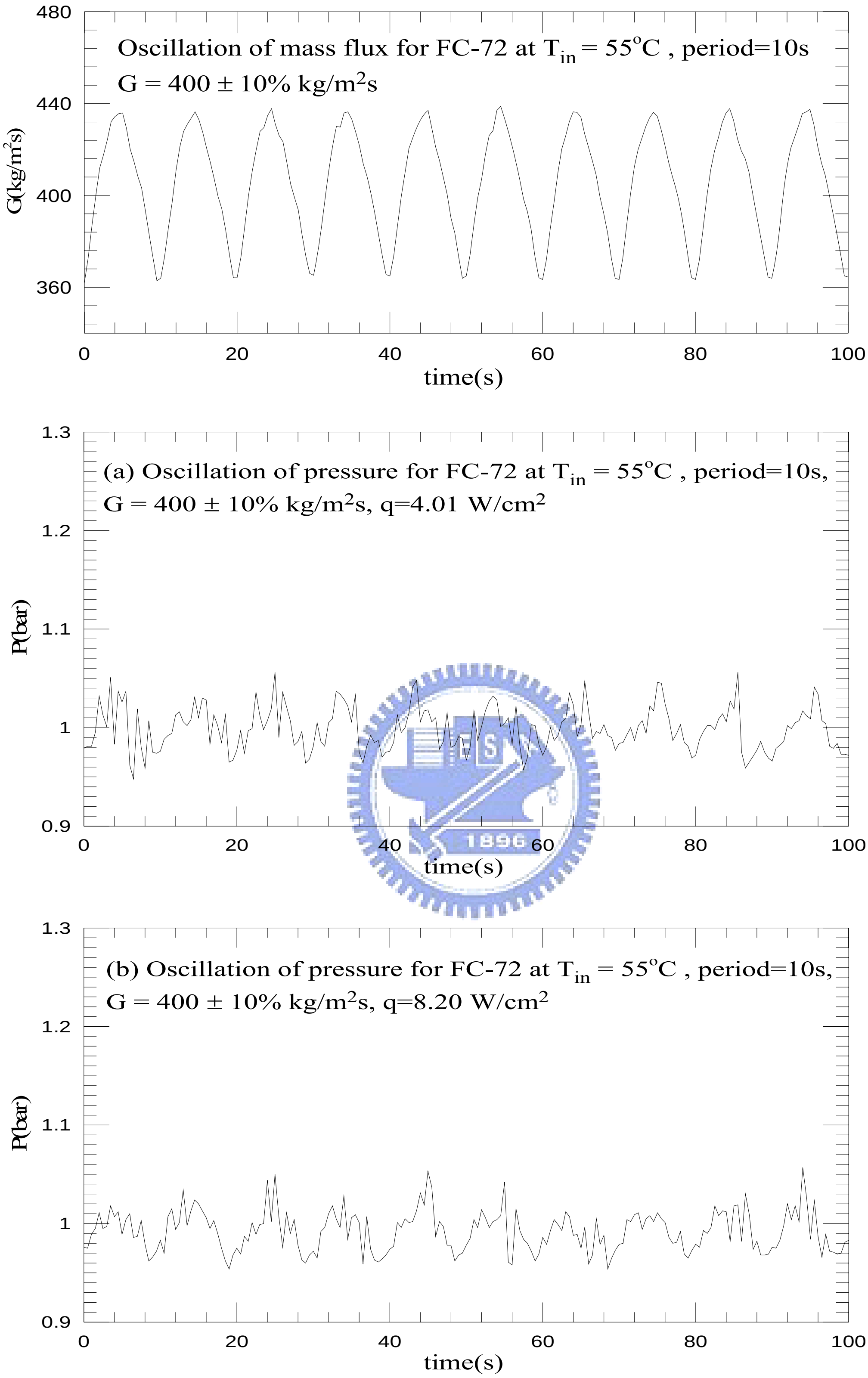

Fig.4.38 Time variations of coolant mass flux and inlet pressure in transient oscillatory saturated flow boiling for various imposed heat fluxes at (a) q=4.01 W/cm^2 and (b) q=8.20 W/cm^2 for G=400±10% kg/m^{2}s with t_p=10 sec.

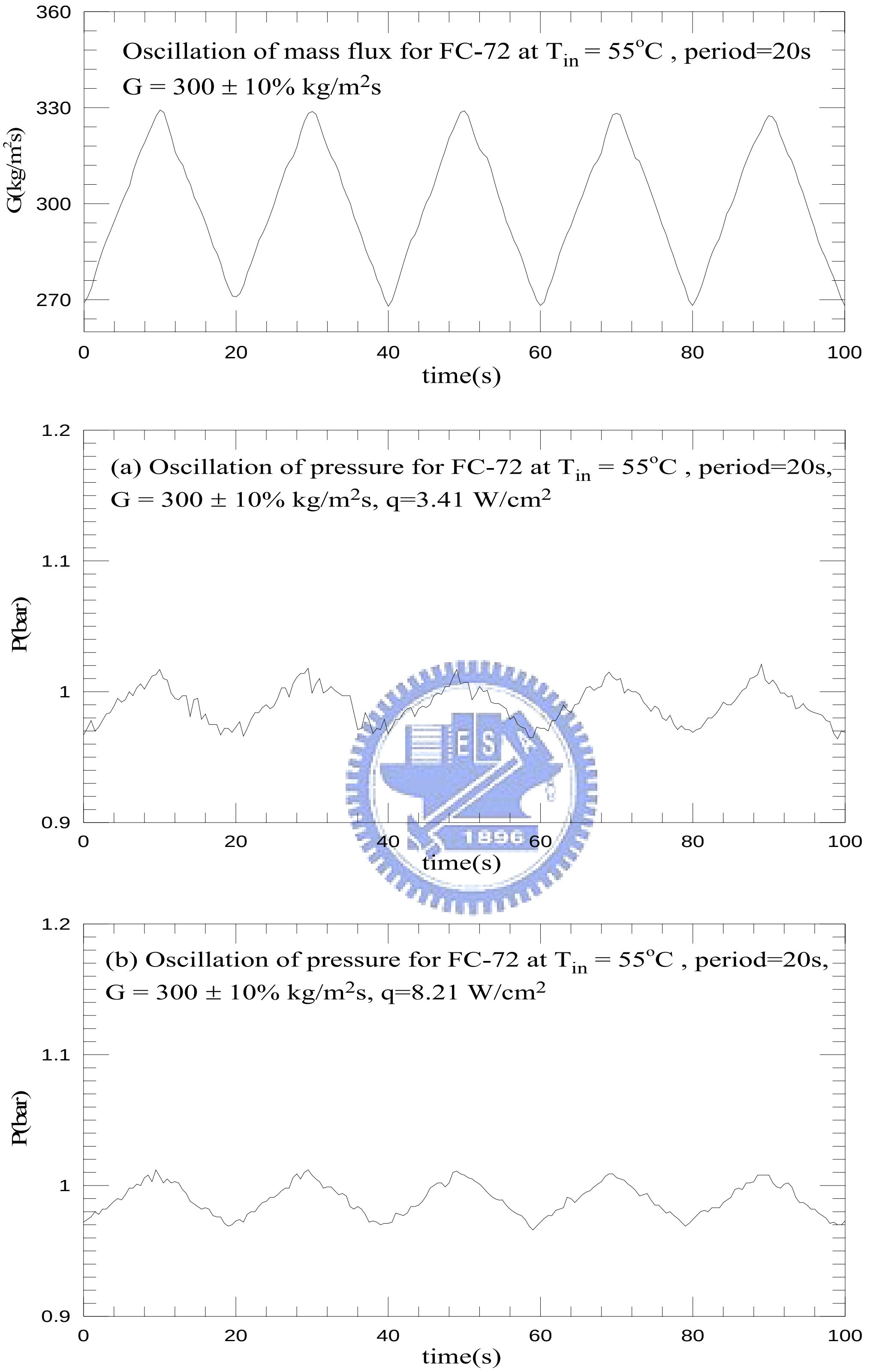

Fig.4.39 Time variations of coolant mass flux and inlet pressure in transient oscillatory saturated flow boiling for various imposed heat fluxes at (a) q=3.41 W/cm^2 and (b) q=8.21 W/cm^2 for G=300±10% kg/m^{2}s with t_p=20 sec.

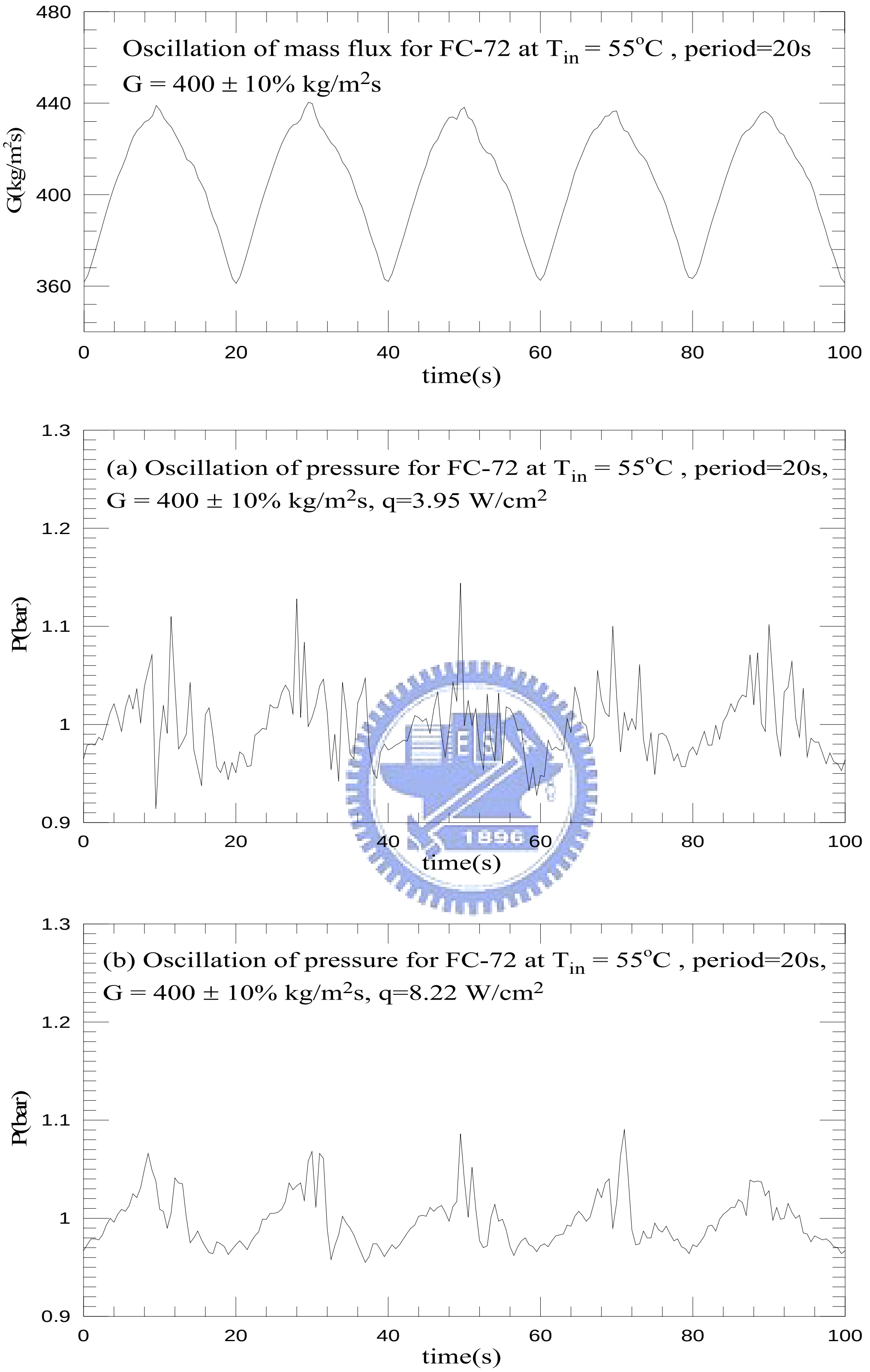

Fig.4.40 Time variations of coolant mass flux and inlet pressure in transient oscillatory saturated flow boiling for various imposed heat fluxes at (a) q=3.95 W/cm^2 and (b) q=8.22 W/cm^2 for G=400±10% kg/m^{2}s with t_p=20 sec.

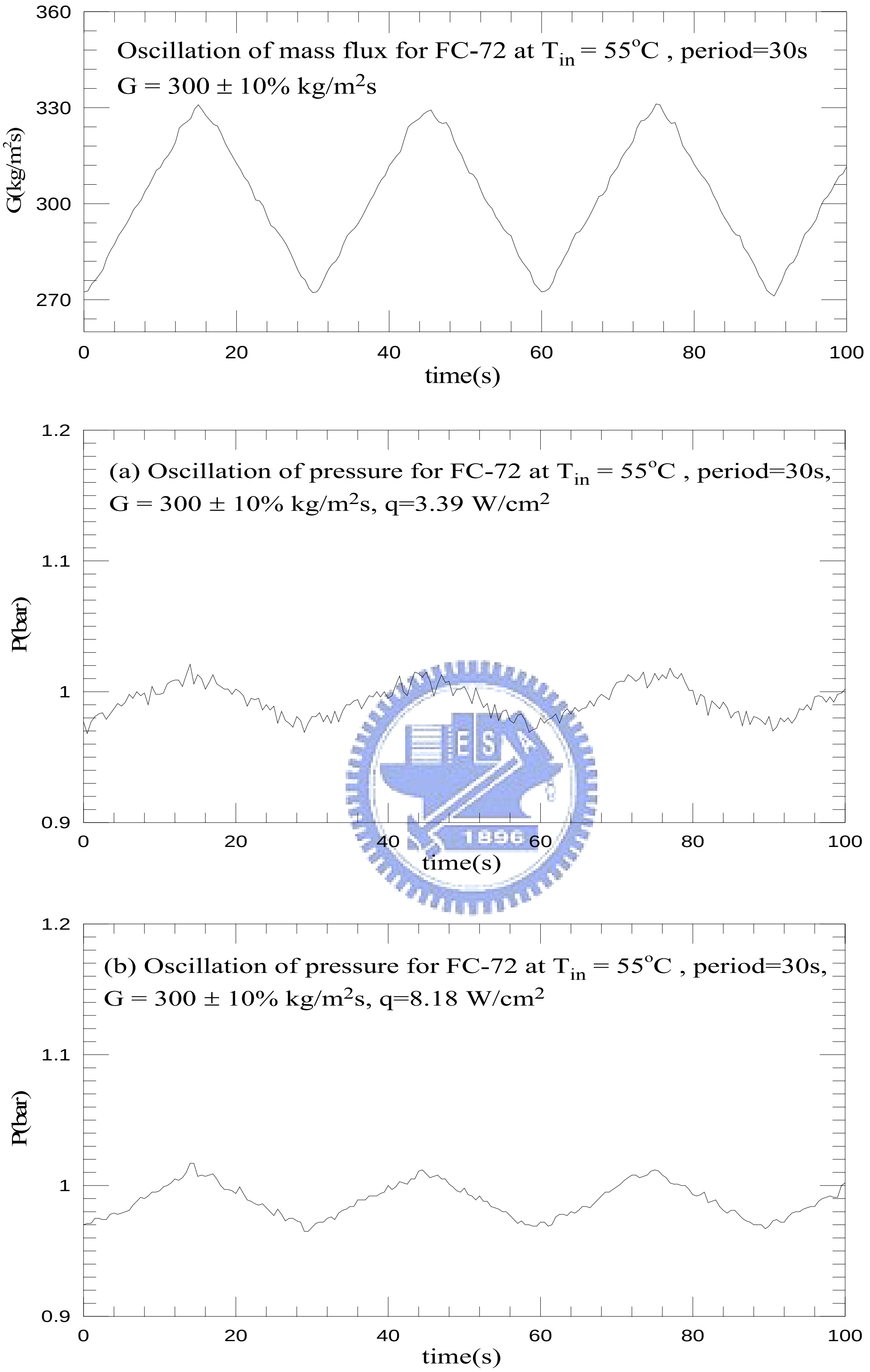

Fig.4.41 Time variations of coolant mass flux and inlet pressure in transient oscillatory saturated flow boiling for various imposed heat fluxes at (a) q=3.39 W/cm^2 and (b) q=8.18 W/cm^2 for G=300±10% kg/m^{2}s with t_p=30 sec.

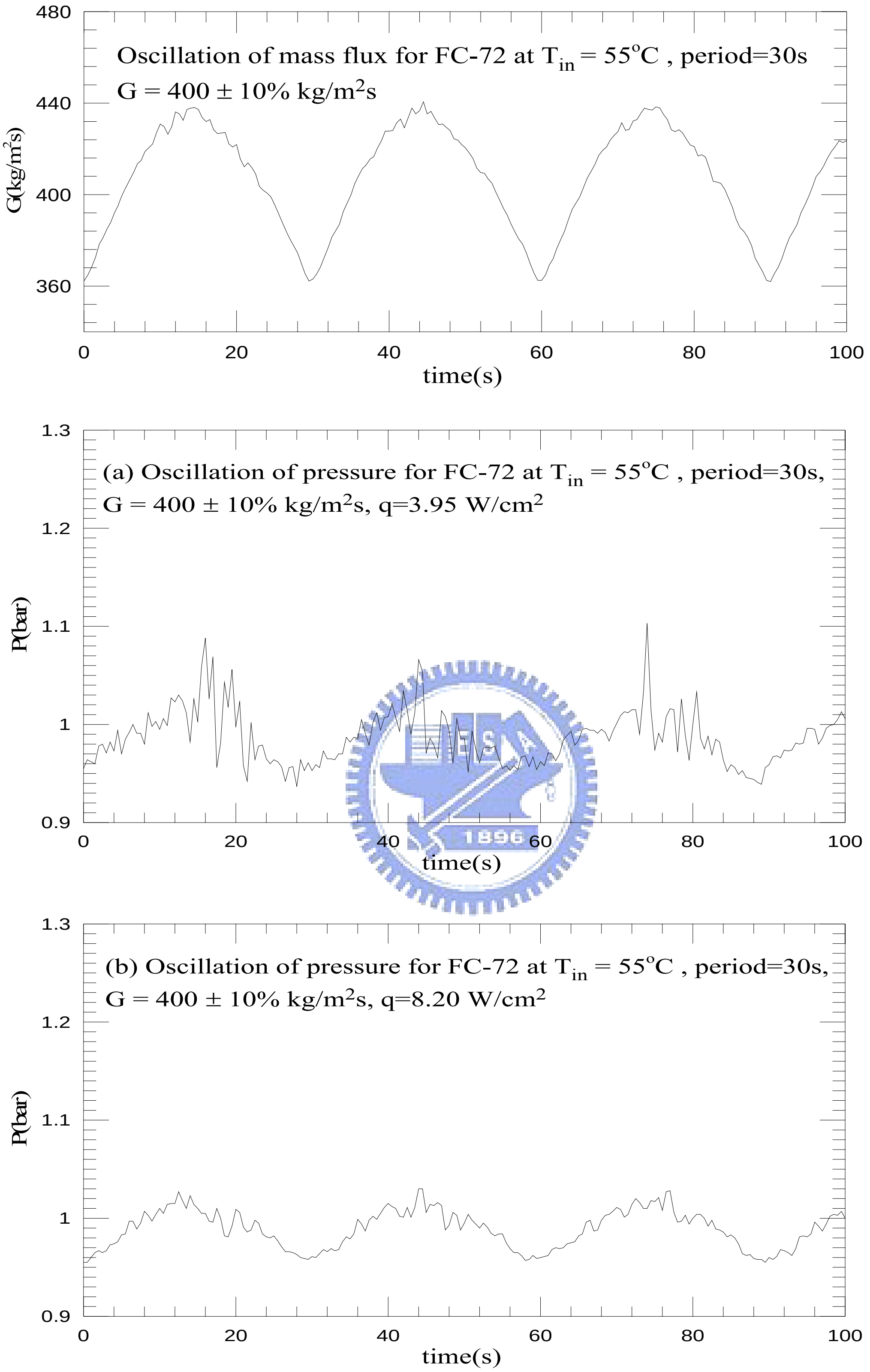

Fig.4.42 Time variations of coolant mass flux and inlet pressure in transient oscillatory saturated flow boiling for various imposed heat fluxes at (a) q=3.95 W/cm^2 and (b) q=8.20 W/cm^2 for G=400±10% kg/m^2s with t_p=30 sec.